# MASTERARBEIT | MASTER'S THESIS

Titel | Title

Investigation of the effect of transient SUMOylation inhibition in human adipocyte progenitors on adipogenesis and DNA methylation in differentiating adipocytes

verfasst von | submitted by

Doris Emely Fröhlich BSc

angestrebter akademischer Grad | in partial fulfilment of the requirements for the degree of

Master of Science (MSc)

Wien | Vienna, 2026

| | |
|---|---|
| Studienkennzahl lt. Studienblatt \| Degree programme code as it appears on the student record sheet: | UA 066 220 |
| Studienrichtung lt. Studienblatt \| Degree programme as it appears on the student record sheet: | Joint-Masterstudium Evolutionary Genomics and Systems Biology |
| Betreut von \| Supervisor: | Univ.-Prof. Dipl.-Biol. Dr. Ulrich Technau |

# Acknowledgement

First of all, I would like to sincerely thank my supervisor at the University of Oslo, Prof. Dr. Pierre Chymkowitch, for the trust he placed in me by giving me the opportunity to work on this project. I am very grateful for the independence I was given as well as for his continuous support throughout the process. His enthusiasm for the topic was truly motivating and made it easy to develop my own interest and excitement for the project. I especially appreciated his honest and prompt feedback, which helped me to critically reflect on my work and continuously improve.

Furthermore, I am especially grateful to Patrizia Nothnagel for her continuous guidance and mentorship. She was not only an excellent mentor but also quickly became a friend and I truly enjoyed the time we spent together both in and outside the lab. Thank you to Paul-Arthur Meslin for his bioinformatics expertise and for helping me better understand and interpret the data, as well as to Damien Dufour for his expertise and for constructively challenging my interpretations.

I would also like to thank my supervisor at the University of Vienna, Prof. Dr. Ulrich Technau, for the uncomplicated collaboration and for his support with all organizational questions and challenges.

Additionally, I am very thankful for my roommate, who always had an open ear for me. Thank you for listening to my concerns, doubts and uncertainties and for all the conversations we shared. The time we spent together made this period not only more enjoyable but also much easier and more light-hearted.

Finally, I would like to thank my friends, family and my partner for their constant support, encouragement and motivation. Thank you for always believing in me, for your patience and for providing both emotional support and much-needed distraction throughout this journey.

# Table of contents

# List of figures

# List of tables

# List of abbreviations

| | |
|---|---|
| 5caC | 5-carboxycytosine |
| 5fC | 5-formylcytosine |
| 5hmC | 5-hydroxymethylcytosine |
| 5mC | 5-methylcytosine |
| ADD | ATRX-DNMT3L-DNMT3A |
| ADPQ | Adiponectin |
| AID | Activation-induced cytidine deaminase |
| ANOVA | Analysis of variance |
| APOBEC | Apolipoprotein B mRNA-editing catalytic |
| BAT | Brown adipose tissue |
| BER | Base excision repair |
| BMI | Body mass index |
| BSA | Bovine serum albumin |
| cAMP | Cyclic adenosine monophosphate |
| CEBPA | CCAAT/enhancer-binding protein α |
| CEBPB | CCAAT/enhancer-binding protein β |
| CEBPD | CCAAT/enhancer-binding protein δ |
| CpG dinucleotide | Cytosine-guanine dinucleotide |
| D | Day |
| DEX | Dexamethasone |
| DNMT | DNA methyltransferase |
| DSBH | Double-stranded β-helical |
| ECL | Enhanced chemiluminescent |
| EM-seq | enzymatic methylation sequencing |
| EMT | Epithelial-mesenchymal transition |
| FABP4 | Fatty acid binding protein 4 |
| FBS | Fetal bovine serum |
| GO | Gene Ontology |
| GWAS | Genome-wide association studies |
| H3K27ac | Histone H3 lysine 27 acetylation |
| H3K27me3 | Histone H3 lysine 27 trimethylation |
| HRP | Horse radish peroxidase |
| HSD | Honest Significant Difference |
| IBMX | 3-Isobutyl-1-methylxanthine |
| IGF | Insulin-like growth factor |
| IQR | Interquartile range |
| MCE | Mitotic clonal expansion |
| MECP2 | Methyl-CpG-binding protein 2 |
| mESC | mouse embryonic stem cell |
| MPHOSPH8 | M-phase phosphoprotein 8 |
| MS | Mass spectrometry |
| OGG1 | 8-oxoguanine DNA glycosylase 1 |
| ORO | Oil Red O |
| $p_{adj}$ | Adjusted p-values |
| PBS | Phosphate-buffered saline |
| PCNA | Proliferation cell nuclear antigen |
| PenStrep | Penicillin/Streptomycin |
| PPARG | Peroxisome proliferator-activated receptor γ |
| PTM | Posttranslational modification |
| PWWP | Pro-Trp-Trp-Pro |

| | |
|---|---|
| Q1 | First quartile |
| Q3 | Third quartile |
| RFTS | Replication foci targeting sequence |
| RNA-seq | RNA sequencing |
| RT | Reverse transcription |
| RT-qPCR | Reverse transcription quantitative polymerase chain reaction |
| SAE1 | SUMO-activating enzyme subunit 1 |
| SAE2 | SUMO-activating enzyme subunit 2 |
| SAM | S-adenosylmethionine |
| SDS-PAGE | Sodium dodecyl sulfate-polyacrylamide gel electrophoresis |
| SENP | SUMO-specific protease |
| SUMO | Small Ubiquitin-like Modifier |
| TBST | Tris-buffered saline with Tween |
| TET | Ten-eleven translocation enzyme |
| TET1FL | Ten-eleven translocation enzyme 1 full-length |
| TET1s | Ten-eleven translocation enzyme 1 short |
| TET3FL | Ten-eleven translocation enzyme 3 full-length |
| TET3s | Ten-eleven translocation enzyme 3 short |
| TET3o | Ten-eleven translocation enzyme 3 oocyte-specific |
| Tm | Melting temperature |
| TPM | Transcripts per million |
| UBC9 | Ubiquitin conjugating enzyme 9 |
| USP7 | Ubiquitin-specific-processing protease 7 |
| WAT | White adipose tissue |

# Abstract

Obesity is a complex multifactorial disease influenced not only by environmental factors but also by genetic and epigenetic mechanisms. SUMOylation, a post-translational protein modification, has been implicated in safeguarding cellular identity and a dysfunctional SUMOylation pathway has recently been shown to restrict adipogenic differentiation, likely through effects on chromatin accessibility and epigenetic regulation. Previous studies suggest that inhibition of SUMOylation expands cell fate potential while inducing global DNA hypermethylation, indicating that SUMOylation may preserve cellular identity by regulating epigenetic factors such as DNA methylation.

This study investigates whether transient hypoSUMOylation prior to adipogenic induction affects adipogenic differentiation and lipid accumulation by modulating DNA methylation dynamics through altered expression of DNA methylation and demethylation enzymes. Human white preadipocytes were treated with the global SUMOylation inhibitor TAK-981 to analyse adipogenic progression, as well as transcriptional and protein dynamics of DNA methyltransferases (DNMTs) and Ten-eleven translocation (TET) family members following transient hypoSUMOylation.

Our results show that transient SUMOylation inhibition enhances adipogenesis and adipogenic transcription. It further reduces DNMT1 gene and protein expression and increases *TET* expression, most notably *TET3*, in the late stage of differentiation. These dynamics likely promote a more open chromatin state, facilitating the activation of adipogenic gene programs and suggesting a mechanistic link between SUMOylation and DNA methylation during adipogenesis.

# Zusammenfassung

Adipositas ist eine komplexe, multifaktorielle Erkrankung, die nicht nur durch Umweltfaktoren, sondern auch durch genetische und epigenetische Mechanismen beeinflusst wird. SUMOylierung, eine posttranslationale Proteinmodifikation, trägt dazu bei, dass die zelluläre Identität aufrechterhalten wird. Gestörte SUMOylierung wurde kürzlich als hemmender Faktor für die adipogene Differenzierung identifiziert. Möglicherweise wird dies durch Veränderungen der Chromatinzugänglichkeit und epigenetische Mechanismen reguliert. Studien deuten darauf hin, dass eine Hemmung der SUMOylierung das Differenzierungspotenzial von Zellen erweitert und gleichzeitig eine globale DNA-Hypermethylierung induziert. Das lässt vermuten, dass SUMOylierung die zelluläre Identität durch Regulation epigenetischer Faktoren wie der DNA-Methylierung bewahrt.

Ziel dieser Arbeit ist es zu untersuchen, ob eine vorübergehende Hemmung der SUMOylierung vor der adipogenen Induktion die adipogene Differenzierung und Lipidakkumulation durch die Anpassung von DNA-Methylierungen durch eine veränderte Expression von DNA-Methylierungs- und Demethylierungsenzymen beeinflusst. Humane weiße Präadipozyten wurden mit dem globalen SUMOylierungsinhibitor TAK-981 behandelt, um in Folge den Verlauf der adipogenen Differenzierung sowie die Transkript- und Proteindynamik von DNA-Methyltransferasen (DNMTs) und Ten-eleven-translocation (TET) Enzymen nach vorübergehender Inhibierung von SUMOylierung zu analysieren.

Unsere Ergebnisse zeigen, dass eine vorübergehende Hemmung der SUMOylierung die Adipogenese und die adipogene Transkription verstärkt. Weiters wird die Gen- und Proteinexpression von DNMT1 reduziert und es kommt zu einer Zunahme der *TET* Expression, insbesondere von *TET3*, im späten Stadium der Differenzierung. Diese Dynamik fördert möglicherweise einen offeneren Chromatinzustand, der die Aktivierung adipogener Genprogramme erleichtert und deutet auf einen mechanistischen Zusammenhang zwischen SUMOylierung und DNA-Methylierung während der Adipogenese hin.

# 1. Introduction

## 1.1. Obesity as a global health challenge

Over the past decades, obesity has emerged as a major global health challenge, driven by increasing food availability, socioeconomic development and profound lifestyle changes in diet, physical activity and behaviour. These shifts, shaped by globalization and industrialized food systems, have driven obesity to pandemic levels (NCD Risk Factor Collaboration, 2024; WHO, 2025). In 2022, more than 890 million adults and over 160 million children and adolescents aged 5-19 years were affected worldwide (WHO, 2025).

Individuals with morbid obesity, commonly defined by a body mass index (BMI) greater than 35 $kg \cdot m^{-2}$, face an increased risk of premature mortality, largely attributable to comorbidities such as cardiovascular disease, type 2 diabetes and certain cancers. More recently, morbid obesity has also been associated with adverse outcomes following SARS-CoV-2 infection (Kitahara *et al.*, 2014; Kalligeros *et al.*, 2020). While environmental determinants play central roles in obesity development, they do not fully account for the pronounced inter-individual variability in fat accumulation, metabolic complications and responses to therapeutic interventions (Locke *et al.*, 2015). This heterogeneity has led to a search for underlying biological mechanisms, particularly those of genetic and epigenetic origin, that influence adipose tissue development, function and plasticity.

## 1.2. Genetic and epigenetic regulation of adiposity

Current studies estimate that approximately 40-70 % of the variability in adiposity-related traits is attributable to genetic influences (Locke *et al.*, 2015, Loos & Yeo, 2022). Genome-wide association studies (GWAS) have identified hundreds of loci associated with BMI, fat distribution and metabolic traits (Locke *et al.*, 2015; Pulit *et al.*, 2019; Loos & Yeo, 2022, Bjune *et al.*, 2025). However, individual effect sizes are generally modest and a substantial proportion of heritability remains unexplained (Locke *et al.*, 2015). Notably, many obesity-associated variants reside in non-coding genomic regions, implicating regulatory mechanisms rather than alterations in protein-coding sequences (Maurano *et al.*, 2012; Finucane *et al.*, 2015). One plausible explanation is that inter-individual differences in the differentiation capacity of adipose stem and progenitor cells into mature, functional adipocytes contribute to the observed phenotypic diversity (Claussnitzer *et al.*, 2015; Emont *et al.*, 2022). Nevertheless, the molecular mechanisms, particularly how chromatin

organization and epigenetic regulation imprint adipogenic potential in adipose stem cells, remain incompletely understood (Hinte *et al.*, 2024). Advancing our mechanistic understanding of epigenetic regulation of adipose tissue formation and function is therefore essential for both fundamental insight and the development of new therapeutic strategies.

## 1.3. Adipose tissue

Adipose tissue is a major endocrine organ that plays a central role in metabolic regulation alongside the liver, muscle, pancreas, gut and kidneys (Shroff *et al.*, 2022). It is a highly heterogeneous tissue composed not only of adipocytes but also of macrophages, fibroblasts, endothelial cells, immune cells and preadipocytes (Chait & den Hartigh, 2020; Harvey *et al.*, 2020).

**Different types of adipocytes**

Adipose tissue heterogeneity is not only driven by diverse cell types, but also by the presence of distinct adipocyte subtypes with specialized functions. All adipocytes originate from mesenchymal stem cells and differentiate via lineage-specific preadipocytes into mature adipocytes (Figure 1). Broadly, three major types of adipose tissue can be distinguished: white adipose tissue (WAT), brown adipose tissue (BAT) and beige adipose tissue. These are named according to their macroscopic appearance, which reflects the characteristics of the adipocytes they contain (Harvey *et al.*, 2020; Rosenwald & Wolfrum, 2013).

WAT is the most abundant form and consists predominantly of white adipocytes. Its primary function is to serve as an energy storage depot by reducing the amount of circulating fatty acids. In addition, WAT has important endocrine functions such as the secretion of hormones and adipokines and plays a key role in maintaining systemic insulin sensitivity. Consequently, WAT is essential for hormonal and metabolic homeostasis (Wronska & Kmiec, 2012). Generally, WAT can be differentiated in metabolically healthy and unhealthy adipose tissue. WAT located subcutaneous, under the skin, is considered metabolically protective and that located in visceral fat deposits, surrounding inner organs, is associated with an increased risk of metabolic diseases. Metabolically healthy tissue is highly vascularised and contains low levels of macrophages (Harvey *et al.*, 2020; Wronska & Kmiec, 2012). Morphologically, white adipocytes are characterized by large unilocular lipid droplets, which account for their whitish appearance and have relatively low mitochondrial content (Gómez-Hernández *et al.*, 2016; Rosenwald & Wolfrum, 2013) (Figure 1).

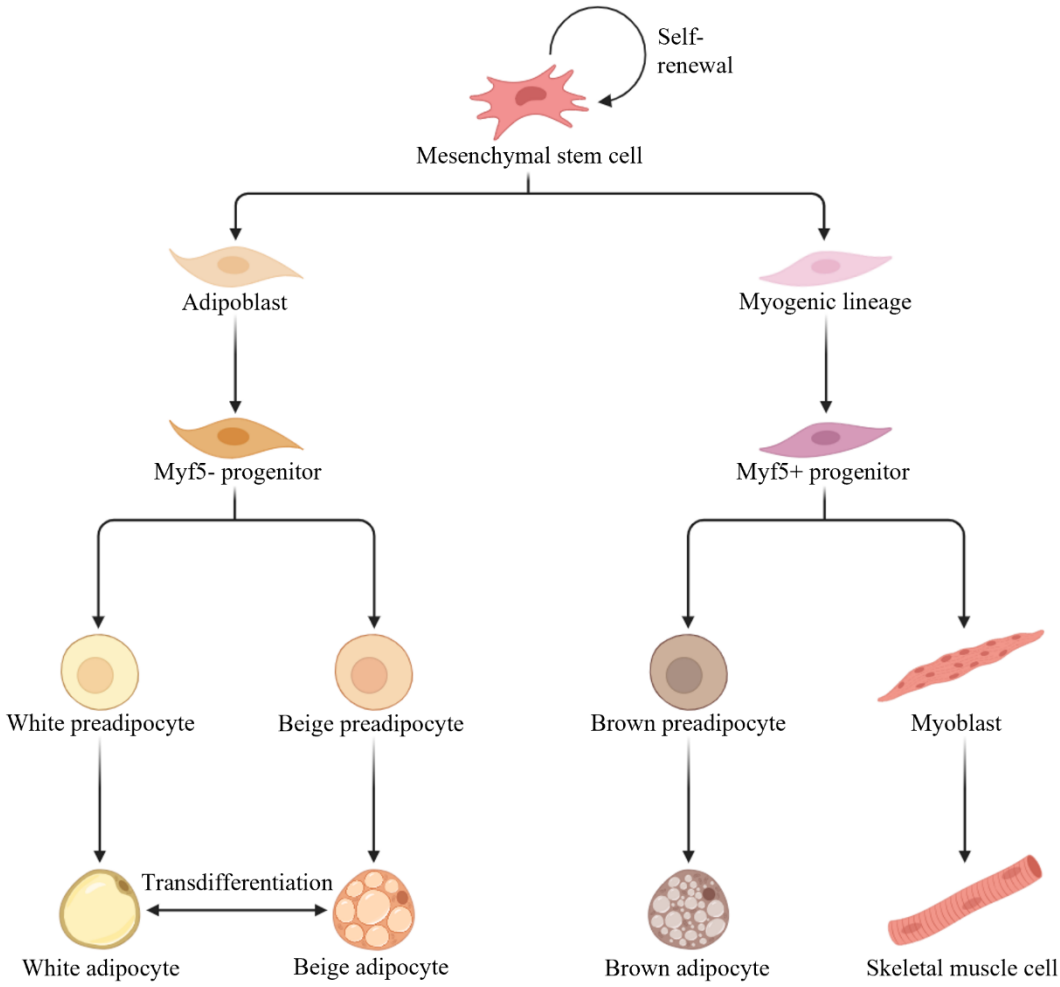


***Figure 1. Origin and differentiation pathways of adipocytes.*** *Mesenchymal stem cells give rise to Myf5⁺ and Myf5⁻ progenitor populations, which differentiate into multiple cell types including preadipocytes. Myf5⁺ progenitors form brown preadipocytes that develop into brown adipocytes, whereas Myf5⁻ progenitors generate white preadipocytes and potentially beige adipocytes. Created with BioRender.com.*

In contrast, BAT represents only 1-2 % of total fat mass in humans and is localised in distinct anatomical regions such as the cervical, axillary and paraspinal areas (Chait & den Hartigh, 2020). Brown adipocytes contain multiple small lipid droplets and a high number of mitochondria, enabling efficient heat production (Figure 1). This process, known as non-shivering thermogenesis, constitutes the primary physiological function of BAT. It involves the uptake of circulating fatty acids and their conversion into heat via UCP1-mediated uncoupling of oxidative phosphorylation. BAT thereby contributes to body temperature regulation (Chait & den Hartigh, 2020; Rosenwald & Wolfrum, 2013). In addition, BAT secretes signalling molecules, termed batokines, including fibroblast growth factors and cytokines, highlighting its endocrine role.

A third adipocyte subtype, referred to as beige adipocytes, emerges within WAT in response to environmental stimuli such as cold exposure, diet or physical activity in a process known as "browning." Beige adipocytes can arise either through transdifferentiation of mature white adipocytes or from dedicated precursor cells, reflecting the remarkable plasticity of adipose tissue. Functionally and morphologically, they resemble brown adipocytes, as they contain multiple small lipid droplets, exhibit increased mitochondrial content and contribute to adaptive thermogenesis (Chait & den Hartigh, 2020; Gómez-Hernández *et al.*, 2016).

**Specific gene expression programs support adipocyte differentiation**

Adipogenesis is a well-characterized process involving tightly coordinated transcriptional and epigenetic programs. *In vitro*, the differentiation of preadipocytes is induced by a defined hormonal cocktail that activates the adipogenic program. This cocktail typically includes a glucocorticoid such as dexamethasone (DEX), 3-Isobutyl-1-methylxanthine (IBMX) to elevate intracellular cyclic adenosine monophosphate (cAMP) levels, insulin to stimulate the insulin receptors and insulin-like growth factor (IGF) receptors, as well as additional growth factors (Siersbæk & Mandrup, 2011, Chang & Kim, 2019). Together, these components initiate a cascade of signalling events that drive the transition from preadipocytes to mature adipocytes (Figure 2).

The early phase of differentiation correlates to the mitotic clonal expansion (MCE) in mice which is characterised by the re-entry of growth-arrested preadipocytes into the cell cycle, resulting in one or two rounds of proliferation during the first two days of differentiation (Chang & Kim, 2019). During this period the transcription factors CCAAT/enhancer-binding protein β and δ (CEBPB and CEBPD) are rapidly induced and act as key early regulators of adipogenesis (Siersbæk & Mandrup, 2011). These factors activate downstream adipogenic master regulators, including peroxisome proliferator-activated receptor γ (PPARG) and CEBPA.

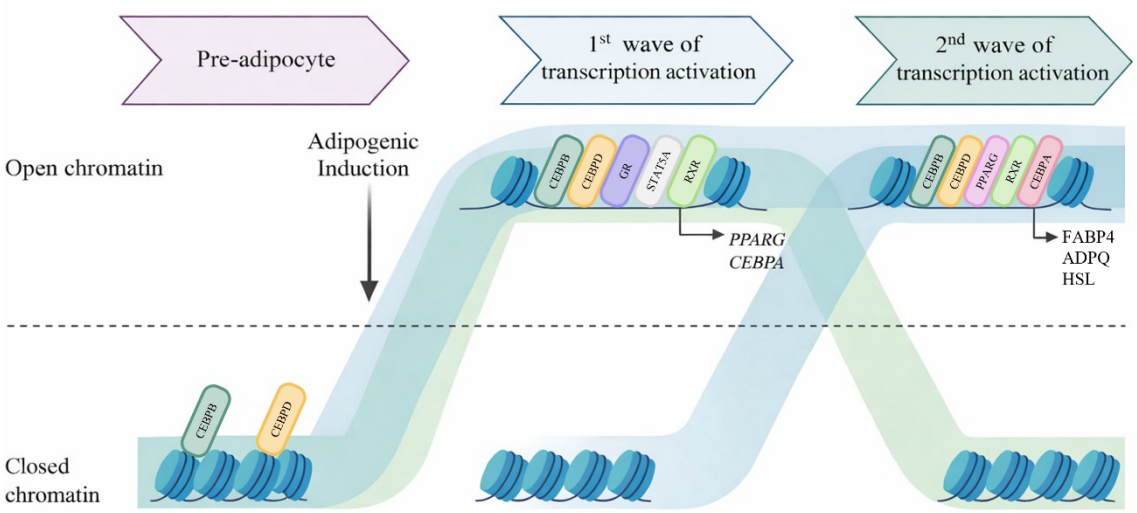


***Figure 2. The transcriptional waves of adipogenesis.*** *Adipogenesis is described to takes place in two waves. During the first wave the early transcription factors of adipogenesis, CEBPB and CEBPD, are upregulated. This is followed by terminal differentiation with specific marker genes upregulated. PPARγ as another central adipogenic transcription factor is highly expressed and upregulates further downstream genes in the late phase of the terminal differentiation. These genes differ depending on the type of adipocyte. Adapted from Lefterova et al., 2014.*

The subsequent upregulation of CEBPA, which brings anti-mitotic effects, marks the completion of MCE and initiates growth arrest, thereby triggering terminal differentiation (Chang & Kim, 2019). Notably, CEBPA expression is characteristic for white adipocyte differentiation (Linhart *et al.*, 2001). Together with PPARG, it drives the expression of adipocyte-specific genes, such as fatty acid binding protein 4 (FABP4), adiponectin (ADPQ) and leptin and establishes the mature adipocyte phenotype throughout the later stages of differentiation (Siersbæk & Mandrup, 2011, Chang & Kim, 2019). The timely coordination and amplitude of adipogenic gene expression networks is controlled by multiple layers of regulation, including posttranslational modifications (PTMs) of gene regulators, including SUMOylation.

## 1.4.SUMOylation pathway

PTMs, which are covalent modifications that occur after RNA has been translated into proteins, are mechanisms extensively widespread in eukaryotes to generate diversity in the proteome (Walsh *et al.*, 2005). Among these PTMs, SUMOylation, the covalent attachment of Small Ubiquitin-like Modifier (SUMO) proteins to lysine residues of target proteins, modulates protein stability, subcellular localisation and protein-protein interactions, thereby reshaping cellular interactomes and regulatory programs (Chymkowitch *et al.*, 2015; Paakinaho *et al.*, 2021).

SUMOylation is a reversible modification that proceeds via a conserved enzymatic cascade (Figure 3). First, immature SUMO precursors are processed by SUMO-specific proteases (SENPs) to expose a C-terminal diglycine motif. Activated SUMO is then transferred to the E1 activating enzyme, a heterodimer of SUMO-activating enzyme subunit 1 and subunit 2 (SAE1/SAE2), conjugated to the E2 enzyme Ubiquitin conjugating enzyme 9 (Ubc9) and finally attached to substrates either directly or with the aid of E3 ligases that confer substrate specificity. The de-SUMOylation is also catalyse by SENPs, maintaining a dynamic equilibrium that is sensitive to cellular contexts (Cubeñas-Potts *et al.* 2013; Sahin *et al.*, 2022).

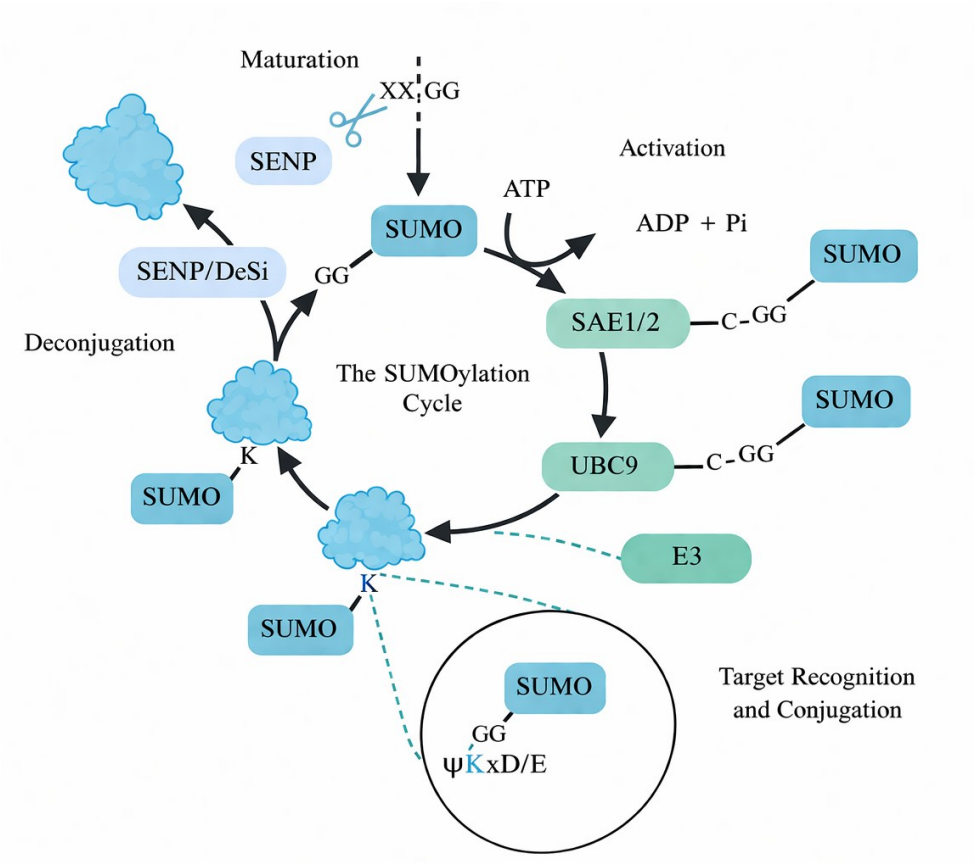


***Figure 3. Overview of the SUMOylation pathway.*** *Schematic representation of the enzymatic cascade of SUMO conjugation, including activation (E1), conjugation (E2) and ligation (E3), as well as deSUMOylation by SENP proteases. Created with BioRender.com.*

In humans, five SUMO paralogs have been described. SUMO1 is structurally distinct, whereas SUMO2 and SUMO3, often referred to collectively as SUMO2/3, are nearly identical and capable of forming polymeric chains that enable complex regulatory signalling (Cubeñas-Potts *et al.* 2013) (Figure 4). SUMO4 and SUMO5 are less well characterised and exhibit restricted expression patterns, suggesting more specialised roles. Together, these

paralogs expand the regulatory repertoire of SUMOylation, allowing cells to fine-tune responses under different physiological and stress conditions.

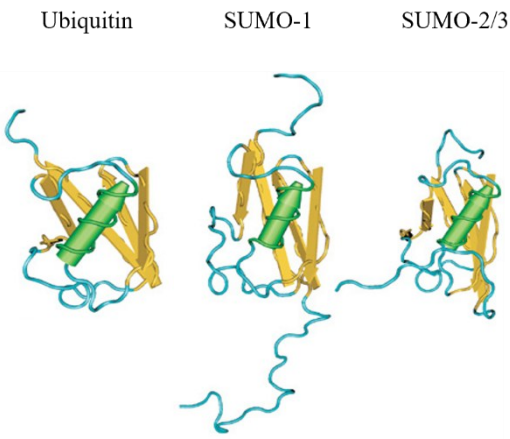


***Figure 4. Structural comparison of ubiquitin and SUMO proteins.*** *Three-dimensional structures of ubiquitin, SUMO1 and SUMO2/3. Reproduced from Martin et al., 2007.*

Over the past decade, SUMOylation has emerged as a key regulator of development, cellular differentiation, cell fate decisions and maintenance of cellular identity (Cossec *et al.*, 2023; Cossec *et al.*, 2018; Demarque *et al.*, 2011; Zhao *et al.*, 2022, Nothnagel *et al.*, 2026). Dysregulation of SUMOylation has been reported in various disease states and is most likely to support cancer stemness and resistance to chemotherapy. Small-molecule SUMOylation inhibitors such as TAK-981 are now in clinical trials, underscoring the therapeutic potential of manipulating this pathway (Seeler & Dejean, 2017; Dudek *et al.*, 2021). Yet, despite its ubiquity and importance, the precise molecular mechanisms regulated by SUMOylation across specific biological contexts remain only partially understood.

To address this, high-throughput proteomic studies, including work from our group, have been conducted. They indicated that approximately 85 % of SUMOylated proteins are localised in the nucleus and participate in chromatin regulation, epigenetic control and transcriptional regulation (Zhao *et al.*, 2022; Rosonina *et al.*, 2017; Baig *et al.*, 2021; Theurillat *et al.*, 2020; Hendriks *et al.*, 2018). These observations are consistent with genetic and biochemical evidence that SUMO orchestrates chromatin remodelling, nucleosome dynamics, transcription factor function and co-regulator assembly. SUMOylation has been shown to preserve the global heterochromatin landscape, thereby suppressing the expression of genes not required for the current cell identity and safeguarding cellular identities. Transient SUMOylation inhibition lifts this repressive barrier and allows for cellular

reprogramming and the adoption of new cell identities (Cossec *et al.*, 2018; Demarque *et al.*, 2011; Zhao *et al.*, 2022; Mikkonen *et al.*, 2013).

## 1.5.SUMOylation in adipogenesis

Adipose tissue development and function appear particularly dependent on an intact SUMOylation pathway both *in vitro* and *in vivo* (Zhao *et al.*, 2022; Mikkonen *et al.*, 2013; Liu *et al.*, 2014; Cox *et al.*, 2021; Bjune *et al.*, 2023; Nothnagel *et al.*, 2026). Studies converge on a central role for SUMO in adipogenic gene transcription, coordinating chromatin dynamics and sustaining lipid homeostasis (Zhao *et al.*, 2022; Sapir, 2020). Preliminary data from our group suggest that SUMOylation in human white pre-adipocytes restrain adipogenic differentiation, thereby preventing excessive fat accumulation (Nothnagel *et al.*, 2026). These findings are consistent with the concept that SUMOylation acts as a safeguard of cellular identity, particularly by maintaining stemness. Moreover, adipogenesis is a well-characterised differentiation system with extensively mapped chromatin and transcriptional dynamics in both human and mouse models, making it an attractive model to investigate SUMO-dependent regulation of epigenetic and transcriptional programs (Zhao *et al.*, 2022; Paulsen *et al.*, 2019; Shah *et al.*, 2014; Siersbæk *et al.*, 2017).

Although the underlying mechanisms by which SUMOylation shapes gene regulation remain to be elucidated, accumulating evidence, including findings from our lab, suggests a link between SUMOylation and epigenetic regulation. Supporting this, transient SUMOylation inhibition in pre-adipocytes has been reported to affect multiple histone marks, suggesting that SUMOylation maintains the epigenetic program of pre-adipocytes and prevents epigenetic drift towards undesired cell identities. These epigenetic changes upon transient SUMOylation inhibition include a reduction of histone H3 lysine 27 trimethylation (H3K27me3) at specific enhancers, indicating that SUMOylation contributes to the maintenance of epigenetic stability. In parallel, increase in histone H3 lysine 27 acetylation (H3K27ac) levels have been detected at similar enhancers, suggesting that SUMOylation represses histone acetylation (Nothnagel *et al.*, 2026). In addition to histone-based mechanisms, SUMOylation has also been linked to the regulation of DNA methylation machinery. Experimental hypoSUMOylation has been shown to not only expand cell fate potential but also alter the epigenetic landscape by inducing global DNA hypermethylation through upregulation of DNA methyltransferases (*Dnmts*) and downregulation of ten-eleven translocation enzymes (*Tets*) in mouse embryonic stem cells (Cossec *et al.*, 2023, Kroonen *et al.*, 2022). Together, these observations point to a broader role of SUMOylation in

coordinating multiple layers of epigenetic regulation, including both histone modifications and DNA methylation, to control gene expression programs and cell fate decisions. In this study, we therefore focus on the effects of SUMOylation on DNA methylation.

## 1.6.DNA methylation

DNA methylation represents one of the most extensively studied epigenetic modifications and plays a fundamental role in maintaining genomic stability, regulating chromatin structure and mediating gene silencing at promoter regions (Denis *et al.*, 2011; Lyko, 2017; Wu *et al.*, 2025, Joshi et al, 2022).

### DNA methylation pathway

In mammals, DNA methylation predominantly occurs at cytosine residues within cytosine-guanine (CpG) dinucleotides, resulting in the formation of 5-methylcytosine (5mC). This reaction is catalysed by DNMTs, which transfer a methyl group from S-adenosylmethionine (SAM) to the C5 position of cytosine (Figure 6) (Lyko, 2017; Wu *et al.*, 2025; Kim, 2025). Structurally, most DNMTs are composed of a N-terminal regulatory domain and a highly conserved C-terminal catalytic domain, which is responsible for enzymatic activity and methyl group transfer (Lyko, 2017; Kim, 2025) (Figure 5).

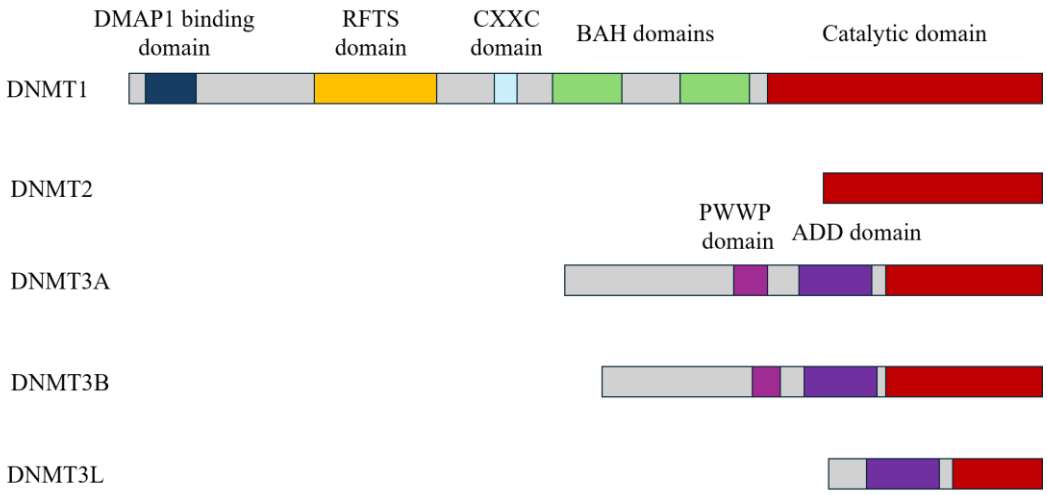


***Figure 5. Structure of DNMT family proteins.*** *Schematic overview of DNMT1, DNMT2, DNMT3 and DNMT3L domain architecture. Adapted from Lyko, 2018.*

Among the five human DNMTs (DNMT1, DNMT2, DNMT3A, DNMT3B and DNMT3L), only DNMT1, DNMT3A and DNMT3B possess catalytic DNMT activity (Lyko, 2017; Wu *et al.*, 2025). DNMT1 primarily functions as a maintenance methyltransferase, preserving existing methylation patterns during DNA replication by preferentially targeting

hemimethylated DNA. This function is facilitated by several regulatory domains within its N-terminus, including the replication foci targeting sequence (RFTS), which directs DNMT1 to replication sites and the proliferation cell nuclear antigen (PCNA) binding domain, which coordinates methylation with DNA synthesis (Lyko, 2017; Kim, 2025). Additional domains, such as the CXXC domain, ensure accurate substrate recognition by binding unmethylated CpG sites, thereby preventing aberrant methylation (Kim, 2025). DNMT1 exists in multiple isoforms, which differ in their N-terminal regions and may exhibit distinct regulatory properties (Kim, 2025).

In contrast, DNMT3A and DNMT3B act predominantly as *de novo* methyltransferases, establishing new methylation patterns on previously unmethylated DNA during development and cellular differentiation (Lyko, 2017; Wu *et al.*, 2025; Kim, 2025). Both enzymes share a similar domain organisation, including a Pro-Trp-Trp-Pro (PWWP) domain that mediates chromatin targeting through recognition of histone marks and an ATRX-DNMT3L-DNMT3A (ADD) domain that interacts with histone tails to regulate enzymatic activity (Kim, 2025). DNMT3A itself exists in at least two isoforms, DNMT3A1 and DNMT3A2 (Kim, 2025). DNMT3B, while functionally overlapping with DNMT3A, shows a preference for methylation of repetitive genomic regions such as centromeric and pericentromeric DNA and is essential for maintaining genomic stability (Kim, 2025).

DNMT2, despite its structural similarity to other DNMTs, exhibits minimal DNA methylation activity and instead primarily functions as a tRNA methyltransferase, highlighting the functional diversification within the DNMT family (Kim, 2025). DNMT3L, on the other hand, lacks catalytic activity but acts as an important regulatory cofactor that enhances the activity of DNMT3A and DNMT3B (Kim, 2025).

Together, the coordinated activity of maintenance and *de novo* DNMTs ensures that DNA methylation patterns are both preserved and newly established when needed. This is important for controlling gene expression, maintaining genomic stability and establishing cell type-specific programs such as adipogenesis.

**DNA demethylation pathways**

DNA demethylation can occur either passively, through inhibition of DNMT activity or actively via enzymatic processes (Wu *et al.*, 2025; Joshi *et al.*, 2022). Active DNA demethylation is mediated by several pathways involving three major enzymatic families (Figure 6). The best-known pathway is the stepwise oxidation of 5mC to 5-

hydroxymethylcytosine (5hmC), 5-formylcytosine (5fC) and 5-carboxycytosine (5caC) by members of the TET family. These oxidised cytosine derivatives are subsequently processed by base excision repair (BER) glycosylases, which mediate DNA repair and restore unmodified cytosines. In addition, the activation-induced cytidine deaminase (AID)/apolipoprotein B mRNA-editing catalytic (APOBEC) family contributes to active DNA demethylation by deamination of 5mC or 5hmC (Wu *et al.*, 2025; Joshi *et al.*, 2022). Among these pathways, TET protein-mediated active DNA demethylation has been studied most extensively and is therefore the primary focus of this work (Wu *et al.*, 2025).

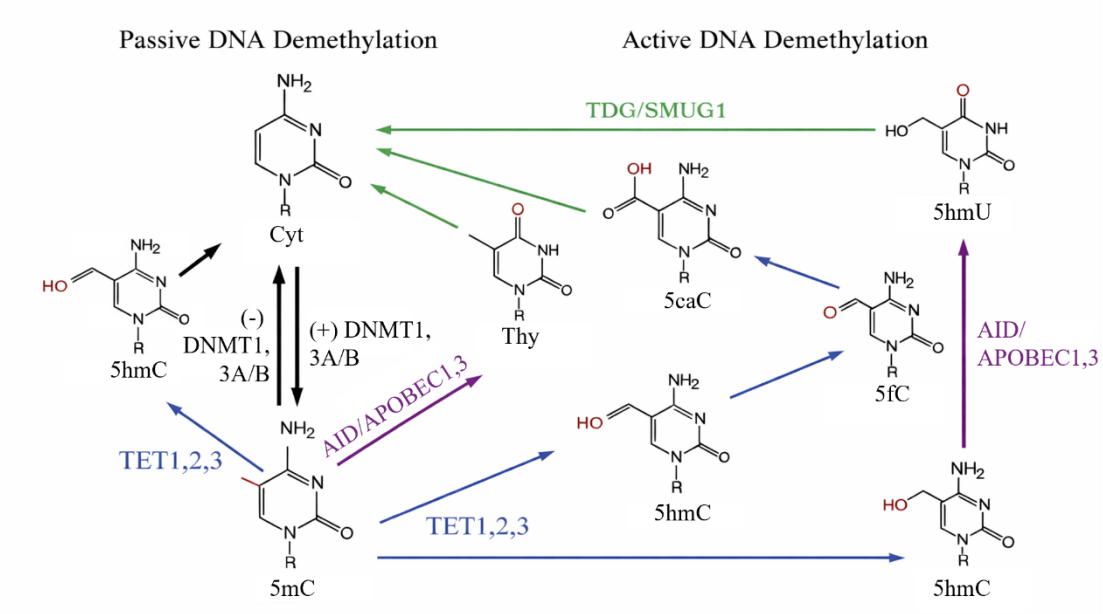


***Figure 6. Mechanisms of DNA demethylation.*** *Schematic overview of active and passive DNA demethylation pathways. Adapted from Bhutani et al., 2011.*

The TET family consists of three members, TET1, TET2 and TET3, all of which contain a carboxyl-terminal catalytic domain comprising a cysteine-rich domain and two double-stranded β-helical (DSBH) regions responsible for their dioxygenase activity (Wu *et al.*, 2025). TET1 and TET3 additionally contain an amino-terminal CXXC domain that mediates binding to CpG-rich DNA regions, whereas TET2 lacks an intrinsic DNA-binding domain and instead relies on interaction partners, such as the CXXC-containing protein IDAX, for genomic targeting (Wu *et al.*, 2025; Joshi *et al.*, 2022) (Figure 7).

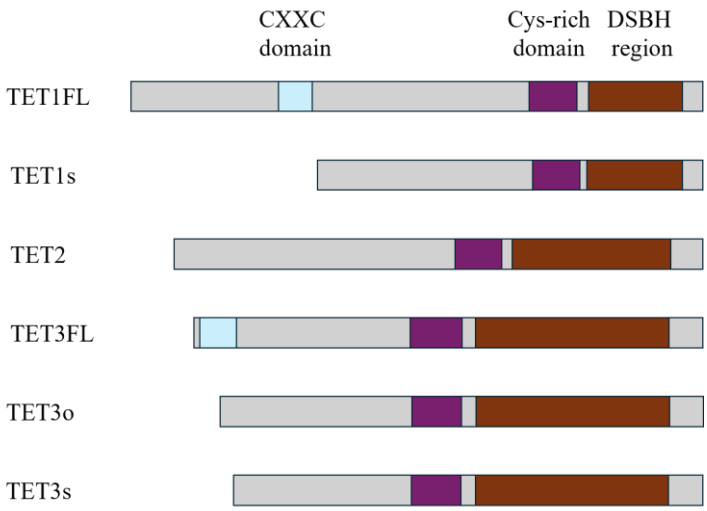


***Figure 7. Structure of TET family proteins.*** *Schematic overview of TET1full-length (FL), TET1short (s), TET2, TET3FL, TET3oocyte-specific (o) and TET3s domain architecture. Adapted from Wu & Zhang, 2017.*

Beyond this shared domain architecture, all three TET genes give rise to multiple isoforms through alternative promoter usage and splicing, adding an additional layer of regulatory complexity. TET1, for instance, is expressed as a full-length isoform (TET1FL) containing the CXXC domain as well as a shorter isoform (TET1s) that lacks most of the N-terminus, including the CXXC domain. While both isoforms retain catalytic activity, they differ in genomic targeting and are differentially expressed across developmental stages, with full-length TET1 predominantly present in embryonic tissues and TET1s in adult tissues (Joshi *et al.*, 2022).

TET2 exhibits even greater isoform diversity, producing multiple variants (TET2-a, TET2-b, and TET2-c) through alternative promoter usage. Only the full-length TET2-b isoform retains catalytic activity, whereas the shorter isoforms lack essential domains and are thought to act as dominant-negative regulators. These isoforms display tissue-specific expression patterns and are dynamically regulated during transitions between pluripotency and differentiation, highlighting their potential role in fine-tuning epigenetic states (Joshi *et al.*, 2022).

Similarly, TET3 exists in several isoforms, including a full-length variant (TET3FL), a shorter isoform (TET3s) lacking parts of the N-terminus containing the CXXC binding domain and an oocyte-specific form (TET3o) described only in mice. These isoforms arise from alternative promoter usage and splicing events. Notably, the full-length and short

isoforms can have distinct and, in some cases, even opposing functions, likely due to differences in their ability to bind specific regulatory regions (Joshi *et al.*, 2022).

Collectively, the existence of multiple TET isoforms with distinct structural features, catalytic capacities and expression patterns suggests that TET-mediated DNA demethylation is regulated not only at the level of gene expression but also through isoform-specific functions.

## 1.7.DNA methylation in adipogenesis

DNA methylation is a key epigenetic mechanism regulating adipocyte differentiation by modulating chromatin accessibility and transcriptional programs. During adipogenesis, dynamic changes in DNA methylation are required to repress stemness-associated genes and activate adipocyte-specific gene expression patterns. These processes are tightly controlled by the coordinated activity of DNMT and TET enzymes (Wu *et al.*, 2025). Studies have demonstrated that the role of DNA methylation during adipogenesis is highly stage dependent. For instance, inhibition of DNA methylation using 5-aza-2′-deoxycytidine has opposing effects depending on the timing of the treatment. While early inhibition in mouse 3T3-L1 preadipocytes suppresses adipogenic differentiation, inhibition at later stages enhances lipogenic gene expression and promotes adipocyte maturation (Yang *et al.*, 2016).

In mouse models, *Dnmt1* displays a distinct expression pattern during adipogenesis, indicating stage-specific functions. *Dnmt1*, the maintenance methyltransferase, is highly expressed in proliferating preadipocytes and during early differentiation, where it preserves existing DNA methylation patterns during DNA replication (Yang *et al.*, 2016, Wu *et al.*, 2025, Cierzniak *et al.*, 2021). As differentiation progresses, *Dnmt1* expression declines, consistent with reduced proliferation and the establishment of a more stable epigenetic landscape in mature adipocytes (Gentile *et al.*, 2013, Yang *et al.*, 2016). In line with this, functional studies have shown that *Dnmt1* depletion has as well time-dependent effects. Inhibition at early stages impairs adipogenesis, whereas inhibition at later stages enhances lipid accumulation and adipocyte maturation (Gentile *et al.*, 2013; Wen *et al.*, 2025).

In contrast, the *de novo* methyltransferases *Dnmt3a* and *Dnmt3b* display less pronounced dynamic regulation during adipogenesis in 3T3-L1 cells. *Dnmt3a* expression remains relatively stable during early stages and shows a slight increase in mature adipocytes, whereas *Dnmt3b* expression is generally low throughout the differentiation process (Yang *et al.*, 2016). Despite these modest expression changes, both enzymes play important

functional roles in adipose tissue biology. Notably, *Dnmt3a* deficiency has been shown to impair adipocyte differentiation and to promote the expression of genes associated with epithelial-mesenchymal transition (EMT), a cellular program linked to increased cell plasticity and loss of epithelial characteristics, highlighting its role in maintaining adipocyte identity (Wu *et al.*, 2025, Wen *et al.*, 2025).

DNA demethylation during adipogenesis is primarily mediated by the TET family proteins (TET1, TET2 and TET3) (Wu *et al.*, 2025). In mouse systems, all three TET enzymes contribute to adipocyte differentiation, as depletion or knockout of individual TET proteins has been shown to impair or block adipogenesis (Qian *et al.*, 2021, Liu *et al.*, 2023, Jung *et al.*, 2023, Wu *et al.*, 2025). Mechanistically, TET proteins facilitate DNA demethylation at regulatory regions of key adipogenic genes, including *CEBP* family members and *PPARG*. This epigenetic remodelling enhances transcriptional activation of adipogenic programs and thereby supports differentiation (Liu *et al.*, 2023, Jung *et al.*, 2023, Wu *et al.*, 2025).

Overall, studies in both mouse and human systems demonstrate that adipogenesis is accompanied by coordinated and stage-specific changes in DNMT and TET expression and activity. These dynamic epigenetic regulators ensure the precise control of gene expression programs required for the transition from preadipocytes to fully differentiated adipocytes.

## 1.8. Crosstalk between SUMOylation and DNA methylation

Global DNA methylation dynamics are tightly regulated by the balance between DNA methyltransferases and enzymes involved in active DNA demethylation pathways (Joshi *et al.*, 2022). Perturbation of this equilibrium has been observed in various cancer types and has also been linked to lipid metabolism disorders, including obesity (Wu *et al.*, 2025; Joshi *et al.*, 2022). The activity of enzymes involved in DNA methylation and demethylation can be regulated at multiple levels. At the protein level, protein-protein interactions and post-translational modifications can modulate the activity of DNMTs and TETs. Notably, studies of the human SUMOylome have identified DNMTs (DNMT1, DNMT3A and DNMT3B) as well as TETs (TET1, TET2 and TET3) as SUMO targets (Hendriks & Nielsen *et al.*, 2017; Hendriks & Nielsen *et al.*, 2018), suggesting direct regulatory crosstalk at the protein level (Denis *et al.* 2011; Liu *et al.*, 2023; Hegde & Joshi, 2021). However, hypoSUMOylation has also been associated with altered expression of *DNMT* and *TET* genes, indicating an additional layer of regulation (Cossec *et al.*, 2023, Kroonen *et al.*, 2022). Together, these

findings highlight a potential regulatory link between SUMOylation and DNA methylation homeostasis, which will be further investigated in this study.

## 1.9. Aim of the project

This project aims to investigate how transient inhibition of SUMOylation prior to adipogenic induction influences adipocyte differentiation and epigenetic regulation. As histone PTMs have been addressed in previous studies in our lab, the present work focuses specifically on the effects of SUMOylation on DNA methylation.

Aim 1: Characterisation of the adipogenic phenotype following transient SUMOylation inhibition

This aim addresses whether transient inhibition of SUMOylation enhances adipogenesis. Preliminary data suggested that hypoSUMOylation promotes adipocyte differentiation, resulting in increased lipid accumulation and elevated expression of adipogenic marker genes. To assess this, lipid accumulation was quantified by Oil Red O (ORO) staining and the expression kinetics of the key adipogenic transcription factor *CEBPA* was analysed over a 21-day differentiation period using reverse transcription quantitative polymerase chain reaction (RT-qPCR).

Aim 2: Analysis of transcriptional changes in DNA methylation machinery in mature adipocytes upon transient SUMOylation inhibition

Previous results indicate a stable overexpression of adipogenic genes following transient SUMOylation inhibition, suggesting epigenetic regulation in response to TAK-981. This aim investigates whether transient hypoSUMOylation alters the expression of genes involved in DNA methylation and demethylation in mature adipocytes. Using previously generated RNA sequencing (RNA-seq) data, differential gene expression was analysed with a focus on DNA methylation and demethylation pathways. This includes the generation of volcano plots for relevant gene ontology terms and isoform-specific analyses of DNMT and TET family members.

Aim 3: Characterisation of DNMT and TET expression dynamics during adipogenesis following transient SUMOylation inhibition

To define the temporal transcriptional and protein-level responses of the DNA methylation machinery, DNMT and TET expression was analysed throughout adipogenic differentiation under TAK-981 treatment and DMSO control conditions. Time-resolved RT-qPCR was

performed to assess gene expression kinetics, while Western blot analysis was used to monitor protein abundance and dynamics across differentiation stages.

Aim 4: Mapping DNA methylation changes during adipogenesis following transient SUMOylation inhibition

This aim explores whether transient hypoSUMOylation leads to genome-wide changes in DNA methylation. To this end, enzymatic methylation sequencing (EM-seq) was performed at selected time points during adipogenesis. This approach enables the identification of differentially methylated regions and provides insight into how SUMOylation influences epigenetic remodelling during adipocyte differentiation.

# 2. Methods

## 2.1. Cell culture, differentiation and treatments

Human white pre-adipocytes (hTERT-A41hWAT-SVF, ATCC, CRL-3386) were maintained and differentiated based on previously established protocols (Herbers *et al.*, 2022; Nothnagel *et al.*, 2026). The differentiation course for the white pre-adipocytes can be divided in three phases: the maintenance phase until day 0 (D0), the differentiation initiation which promotes the adipogenic induction from D0 to D7 and the differentiation phase from D7 onwards.

Cells were amplified in StableCellTM DMEM High Glucose Medium (Sigma, D0819), supplied with 10 % Fetal Bovine Serum (FBS, F7524) and 1 % Penicillin/Streptomycin (PenStrep, Gibco, 15140-122), at 37 °C in a humidified incubator at 5 % $CO_2$ in air atmosphere. In advance to differentiation induction, the pre-adipocytes were grown to full confluence (D-2) and maintained at full confluency for another two days. The global SUMOylation inhibitor TAK-981 (Takeda, HY-111789) was administered at 0.5 µM working concentration and DMSO as vehicle control at D-2 for 48 hours. After treatment, cells were washed with phosphate-buffered saline (PBS) and adipogenic differentiation was induced by adding StableCellTM DMEM High Glucose Medium supplied with 2 % FBS, 1 % PenStrep, 1 µM dexamethasone (D4902, Sigma), 0.5 mM IBMX (I5879, Sigma), 0.1 µM human insulin (91077C, Sigma), 17 µM pantothenate (5155, Sigma), 22 µM biotin (B4639, Sigma) and 1 µM rosiglitazone (R2408, Sigma) for 7 days. For time courses extending beyond this 7-day induction phase, the induction medium was replaced with maintenance medium, consisting of StableCellTM DMEM High Glucose Medium supplemented with 2 % FBS, 1 % PenStrep, 1 µM dexamethasone, 0.1 µM human insulin, 17 µM pantothenate and 22 µM biotin for the remainder of the experiment. The medium was refreshed every second or third day.

## 2.2. RNA-seq analysis

RNA-seq has been performed on differentiated human white pre-adipocytes (hTERT-A41hWAT-SVF, ATCC, CRL-3386) as published before (Nothnagel *et al.*, 2026). In brief, cells have been cultured and differentiated as described in “Cell culture, differentiation and treatments”. At D21, RNA was extracted using TRIzol Reagent (15596018, Invitrogen) as described in “RNA extraction”. The RNA was then cleaned with a RNeasy Mini Kit (74104, Qiagen) and sent for sequencing. The processed RNA-seq data were used to investigate

differential expression of genes involved in DNA methylation and demethylation in mature adipocytes.

**Gene ontology analysis**

Gene-level expression values were obtained from the provided RNA-seq dataset, including log2 fold changes and multiple-testing adjusted p-values for the comparison between TAK-981-treated and DMSO control samples. Genes associated with DNA methylation and demethylation were identified based on Gene Ontology (GO) annotations. Specifically, genes annotated to the GO terms "negative regulation of gene expression via chromosomal CpG island methylation" (GO:0044027) and "positive regulation of gene expression via chromosomal CpG island demethylation" (GO:0044029) were selected. GO annotations for human genes were obtained from the Gene Ontology database AmiGO 2 (Ashburner *et al.*, 2000; The Gene Ontology Consortium, 2026; Carbon *et al.*, 2009) on the 18th of February and matched to gene identifiers present in the RNA-seq dataset. Only genes with valid GO annotations were retained for downstream analyses. Data processing, filtering and visualisation steps were performed using RStudio 4.3.1 (R Core Team, 2025).

**Gene expression analysis for *DNMTs* and *TETs***

For a more detailed view of *DNMT* and *TET* expression levels in cells treated with TAK-981 or DMSO, normalised expression values in transcripts per million (TPM) were extracted from the analysed RNA-seq dataset. These values were visualised in bar plots, with asterisks indicating statistically significant differences between the two conditions. Significance was determined based on adjusted p-values obtained from the provided dataset. Data visualisation was performed using RStudio 4.3.1 (R Core Team, 2025).

**Isoform analysis for *DNMTs* and *TETs***

For the isoform analysis, the RNA-seq data were reanalysed starting from the original FASTQ files to obtain information on the expression of individual transcripts of the *DNMT* and *TET* genes. The nf-core/rnaseq 3.22.0 pipeline (Ewels et al, 2020) was used for the analysis, with Salmon v1.10.3 (Patro et al, 2017) employed as a pseudo-aligner. For annotation, the GENCODE Release 38 (GRCh38.p13) reference genome was used. The TSV output file was further analysed using Sleuth 0.30.2 (Pimentel *et al.*, 2017). This isoform analysis was carried out with the support of our group's bioinformatics postdoc, Paul-Arthur

Meslin. Downstream processing, filtering, and visualisation were performed using RStudio 4.3.1 (R Core Team, 2025).

## 2.3. Mass spectrometry analysis

To obtain information on DNMTs and TETs as potential SUMO targets, mass spectrometry (MS) data from several published studies were analysed (Zhao *et al.*, 2022; Cossec *et al.*, 2023; Hendriks *et al.*, 2017; Hendriks *et al.*, 2018; Theurillat *et al.*, 2020; Goffeney *et al.*, 2025). Data visualisation was performed using RStudio 4.3.1 (R Core Team, 2025).

## 2.4. ORO staining

ORO staining was used to selectively visualise neutral lipids, predominantly triglycerides stored in cytosolic lipid droplets. This selectivity is based on the reduced solubility of the dye in the dye solution than in the neutral lipids, causing the hydrophobic dye to dissociate from the solvent phase and bind preferentially to neutral lipids within lipid droplets (Du *et al.*, 2023). This approach was employed to identify putative white adipocytes based on their prominent lipid droplet accumulation compared with preadipocytes and other cell types. Cells were fixed and stained using the Lipid (Oil Red O) Staining Kit by Sigma-Aldrich. Lipid droplets were stained red with Oil Red O and nuclei were counterstained blue with hematoxylin, following the manufacturer's protocol with the modification that 10 % formaldehyde was used instead of 10 % formalin as the fixative. Stained cells were analysed using a benchtop light microscope and various magnifications. Images were taken with a regular camera.

## 2.5. RT-qPCR

To define early to late transcriptional responses of the DNA methylation machinery to transient hypoSUMOylation prior to adipogenesis, *DNMT* and *TET* expression was analysed during adipogenic differentiation following the TAK-981 treatment and DMSO control treatment as described in "Cell culture, differentiation and treatments" using RT-qPCR. RT-qPCR analyses were performed at days −2, 0, 0.5 1, 2, 3, 7, 14 and 21. Total RNA was extracted from TAK-981- and DMSO-treated cells at respective time points during adipogenesis, using three biological replicates per condition. Gene expression was assessed for *DNMT1, DNMT3A, DNMT3B, TET1, TET2,* and *TET3* using specifically designed primer sets.

**Primer design**

Primer sets were designed to quantify the expression of key enzymes involved in DNA methylation and demethylation during adipogenic differentiation. Therefore, the focus was placed on the DNA methyltransferases DNMT1, DNMT3A and DNMT3B, which are responsible for establishing and maintaining DNA methylation patterns and possess catalytic activity and on the TET family members TET1, TET2 and TET3, which are essential mediators of the first step of active DNA demethylation through oxidation of 5-methylcytosine (Wu *et al.*, 2025; Joshi *et al.*, 2022).

For those selected targets, primers were designed to specifically detect nascent RNA to obtain an accurate estimate of transcriptional activation at defined time points. To this end, primers spanning intron-exon junctions were generated, thereby preferentially amplifying unspliced transcripts. Gene structures were examined using the UCSC Genome Browser (Kent *et al.*, 2002) and exon-intron boundaries present in as many transcript isoforms as possible were selected. Corresponding genomic sequences were retrieved from UCSC and used to design suitable primer pairs with the PrimerQuest Tool (Integrated DNA Technologies, 2026). Primer candidates were selected based on amplicon size, coverage of the junction region, melting temperature (Tm) and GC content. Primer specificity was subsequently validated *in silico* using NCBI Primer-BLAST (Ye *et al.*, 2012), ensuring that each primer pair selectively amplified the intended target with high transcript coverage.

In addition to self-designed primers, primer pairs were adopted from published studies in which they had been experimentally validated. For DNMT genes, exon-exon junction primers were obtained from Liao, J. *et al.*, 2015 and for TET genes, primers targeting exonic regions were used based on Xu, Y. *et al.*, 2020.

Lastly, a previously designed primer for CEBPA was used to assess the differential expression of an adipogenic marker.

Amplification efficiencies of all primer pairs were assessed using standard curve analyses based on serial cDNA dilutions. All primer sequences used in this study are listed in Table S1 and the amplification regions of the *DNMT* and *TET* primers are illustrated in Figure 8.

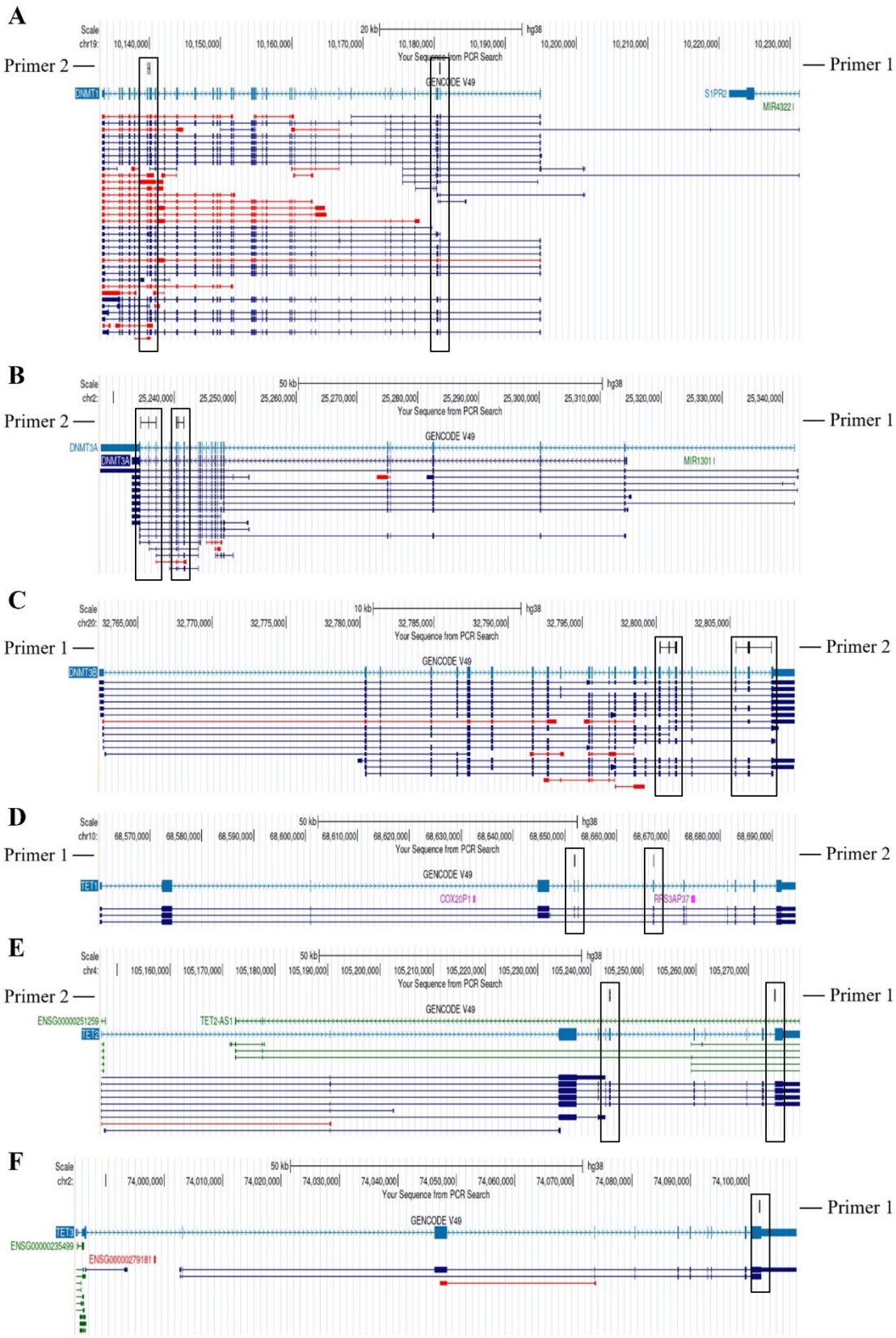


***Figure 8. Primer amplification sites and transcript variants of DNMT and TET genes.*** *Schematic representation of primer binding locations and transcript variants for (A) DNMT1, (B) DNMT3A, (C) DNMT3B, (D) TET1, (E) TET2 and (F) TET3.*

**RNA extraction**

Cells were grown, treated and differentiated as described in "Cell culture, differentiation and treatments" in 12-well plates. For the short kinetic experiment RNA was extracted at day 2, 0, 0.5, 1, 2, 3 and 7 using TRIzol. On the day of collection, cells were washed twice with PBS and lysed directly in 500 µL TRIzol Reagent (15596018, Invitrogen) per well of a 12-well plate. Samples were stored in TRIzol at −80 °C until the final collection day, after which RNA extraction was carried out simultaneously for all samples to minimise variability.

For extraction, samples were vortexed thoroughly, incubated on ice for 5 minutes and centrifuged at 13,200 RPM for 10 minutes at 4 °C. The aqueous phase containing RNA was transferred to a new RNase-free tube, the RNA was precipitated with 100 % isopropanol and incubated on ice for 5 minutes. After centrifugation at 13,200 RPM for 10 minutes at 4 °C, the supernatant was discarded and the RNA pellet washed with 70 % ethanol. The pellet was then centrifuged again at 13,200 RPM for 5 minutes at 4 °C, briefly air-dried and resuspended in RNase-free water. The samples were incubated on ice for 20 minutes to ensure complete dissolution. RNA concentration was determined using a NanoDrop 3000 spectrophotometer (Nothnagel *et al.*, 2026).

**Reverse Transcription**

For the reverse transcription (RT) of the extracted RNA the Qiagen Reverse transcriptase Kit (Qiagen, 205313) was used according to the manufacturer's protocol. For each sample 1 µg of RNA was used in the reaction. The resulting cDNA was stored at -20 °C for further use.

**Reverse Transcription quantitative Polymerase Chain Reaction**

RT-qPCR was performed using the HOT FIREPol® EvaGreen® qPCR Supermix (08-36-00001-5, Solis Biodyne) on a LightCycler 96 instrument (Roche Diagnostics). For each reaction a 1:5 dilution of cDNA and was prepared according to Table 1. A serial dilution of cDNA (1:4, 1:20, 1:100, 1:500) was included to assess amplification efficiencies for each primer. All samples and controls were analysed in technical duplicates.

| Reagents | Volume added [µL] |
|---|---|
| Primer (10 µM, forward and reverse) | 0.2 |
| qPCR Supermix | 2 |
| MilliQ-H2O | 5.8 |
| Diluted cDNA (1:5) | 2 |
| Total | 10 |

***Table 1. RT-qPCR reaction mix.*** *Composition of the reaction mix per well, including reagent volumes and concentrations.*

The following amplification program was run on the qPCR machine:

| Step | | Description [°C] | Time [s] | Cycles |
|---|---|---|---|---|
| Denaturation | | 95 | 720 | 1 |
| 3 Step Amplification: | Denaturation | 95 | 15 | 45 |
| | Primer annealing | 58 | 20 | |
| | Primer extension | 72 | 20 | |
| Melting curve protocol | | 95 | 10 | 1 |
| | | 65 | 60 | |
| | | 97 | ∞ | |

***Table 2. RT-qPCR thermocycler program.*** *Stepwise thermal cycling protocol used for quantitative RT-qPCR.*

## Statistical analysis

RT-qPCR data were analysed using the comparative $2^{-\Delta\Delta Ct}$ method to determine relative gene expression changes during adipogenic differentiation (Livak & Schmittgen, 2001). Ct values were obtained for each target gene and normalised to the housekeeping gene *18S rRNA*, which served as an internal control due to its stable expression across all differentiation stages and treatment conditions (Catalán *et al.*, 2007).

For each sample, the ΔCt value was calculated as the difference between the Ct value of the target gene and the Ct value of *18S rRNA*: $\Delta Ct = Ct_{target} - Ct_{18S}$

To assess relative expression changes over time, the time point D−2 was used as the baseline reference. The ΔΔCt value was calculated by subtracting the ΔCt of the reference sample (D−2) from the ΔCt of each experimental sample: $\Delta\Delta Ct = \Delta Ct_{sample} - \Delta Ct_{D-2}$

Relative gene expression levels were then determined using the following formula: $2^{-\Delta\Delta Ct}$

This approach allowed quantification of gene expression relative to the baseline stage before adipogenic induction. To minimise the influence of technical variability, outliers were removed prior to statistical analysis using the interquartile range (IQR) method (Vinutha *et al.*, 2018). Relative expression values were grouped by time point and treatment condition.

For each group, the first quartile (Q1) and third quartile (Q3) were calculated and the IQR was defined as: $IQR = Q3 - Q1$

Values lying below $Q1 - 1.5 \cdot IQR$ or above $Q3 + 1.5 \cdot IQR$ were considered outliers and excluded from further analysis. This procedure ensured robust comparison of expression levels across differentiation stages.

Statistical significance of gene expression differences between TAK-981- and DMSO-treated cells was assessed using a two-way analysis of variance (ANOVA). Following ANOVA, Tukey's Honest Significant Difference (HSD) post-hoc test was applied to correct for multiple comparisons and to identify significant differences between treatment and control conditions at each individual time point. Adjusted p-values ($p_{adj}$) were extracted specifically for comparisons between TAK-981 and DMSO groups within the same differentiation stage. Any difference with a $p_{adj}$ of 0.05 or less was considered to be statistically significant ($*$ $p < 0.05$, 756 $**$ $p < 0.01$, $***$ $p < 0.001$ and $****$ $p < 0.0001$). Statistical analysis and data visualisation was performed using RStudio 4.3.1 (R Core Team, 2025).

## 2.6. Western blotting

Protein-level dynamics of DNMTs and TETs in response to transient hypoSUMOylation prior to adipogenesis were analysed at days -2, 0, 0.5, 1, 2, 3, 7, 14 and 21 post adipogenic induction using Western blots.

### Protein extraction

Cells were grown, treated and differentiated as described in "Cell culture, differentiation and treatments" in 12-well plates. Cells were harvested and united from two wells per condition and time point. After washing twice with ice-cold PBS, cells were lysed in 100 µL ice-cold adipocyte lysis buffer (Durcin *et al.*, 2017), freshly supplemented with protease inhibitor cocktail (4693159001, Roche) and 0.1 % β-mercaptoethanol. Cell lysates were homogenised by shearing the samples five times with a 26G needle, followed by centrifugation at 11,000 rpm for 10 minutes at 4 °C and were stored at −80 °C until all samples were further processed.

**SDS-PAGE and protein transfer**

Protein concentrations were determined using a Bradford assay. Concentrations were calculated based on a bovine serum albumin (BSA) standard curve that was prepared by diluting BSA in milliQ $H_2O$. For the sodium dodecyl sulfate-polyacrylamide gel electrophoresis (SDS-PAGE) 20-40 µg of total protein per sample were prepared by mixing the lysates with 4x Laemmli buffer and adjusting the final volume with lysis buffer to obtain a 1x working concentration. Samples were denatured at 95 °C for 5 minutes before loading onto the gel.

Proteins were separated using precast 4-15 % gradient gels (Bio-Rad) in 1x SDS running buffer (prepared from a 10x stock solution). A molecular weight marker was loaded alongside the samples. Electrophoresis was performed at 80V for the first 20 minutes and was then set to 120 V until the dye front reached the bottom of the gel.

Following separation, proteins were transferred onto a 0.2 µm nitrocellulose membrane using the Bio-Rad Trans-Blot Turbo system. Membranes, gels and Whatman filter papers were equilibrated in cold 1x transfer buffer for 5 minutes. Transfer was carried out using the high molecular weight protocol for mini of midi format gels respectively (10 minutes, 1.3 A/2.5 A, up to 25 V).

**Immunodetection**

Membranes were blocked in 5 % non-fat milk prepared in 1x Tris-buffered saline with Tween (TBST) for 1 hour at room temperature to prevent non-specific antibody binding. Subsequently, membranes were incubated overnight at 4 °C with primary antibodies diluted in 5 % non-fat milk in 1x TBST according to the manufacturer's recommendations.

After incubation, membranes were washed three times for 5 minutes each in 1x TBST and then incubated with horse radish peroxidase (HRP)-conjugated secondary antibodies in 5 % non-fat milk in 1x TBST for 1 hour at room temperature. Membranes were washed again three times in 1x TBST before protein bands were visualised using an enhanced chemiluminescent (ECL) substrate and detected with a BioRad chemiluminescence imaging system.

Western blotting was performed to detect the epigenetic regulators DNMT1, DNMT3A, DNMT3B, TET1, TET2 and TET3. γ-Tubulin was used as a loading control (Table S2).

## 2.7. Enzymatic methylation sequencing

Global DNA methylation patterns were profiled by EM-seq in samples collected at days −2, 0, 0.5 and 7 following treatments with TAK-981 and under control conditions.

**DNA extraction**

Cells were grown as described in „Cell culture, differentiation and treatment“ in 12-well plates as triplicates. Genomic DNA and RNA was isolated from cell samples collected at day −2, 0, 0.5, 1, 2, 3, 7, 10, 14 and 21. On each collection day, cells were washed twice with PBS and lysed directly in 200 µL 1X DNA/RNA Shield (R2130, Zymo Research) per well of a 12-well plate. Lysates were stored in 1X DNA/RNA Shield at 4 °C until the final collection day.

DNA and RNA were extracted separately using the Quick-DNA/RNA MagBead Kit (Zymo Research), following the manufacturer's instructions. Extracted DNA was quantified using the Qubit 4 Fluorometer (Q33226, Invitrogen) and stored at -20 °C until library preparation for EM-seq. RNA was quantified using a NanoDrop spectrophotometer and samples with a sufficiently high concentration (> 800 ng/12 µL) were reverse transcribed and used for the 21-day RT-qPCR kinetics (see Methods section "Reverse transcription" and "Reverse Transcription quantitative Polymerase Chain Reaction").

**DNA fragmentation**

Genomic DNA was fragmented to an average size of approximately 350 bp using a Diagenode Pico Sonicator in accordance with the recommendations of the NEBNext Enzymatic Methyl-seq v2 Kit (NEB-E8015S, New England Biolabs). To determine optimal sonication conditions, test runs were performed and fragment size distributions were assessed by agarose gel electrophoresis using Orange G as loading dye. Ten sonication cycles were identified as optimal when using 0.2 mL sonication tubes (C30010020, Diagenode), with 30/30 s on/off cycling and a sample volume of 50 µL (Figure 9).

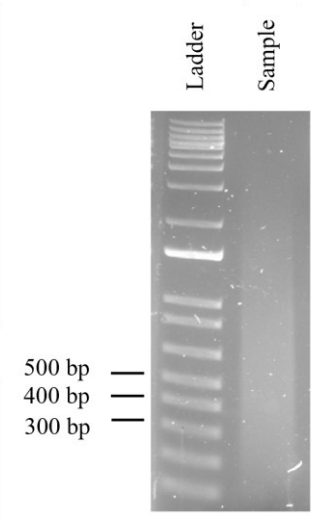


***Figure 9. DNA fragmentation for library preparation.*** *Agarose gel electrophoresis showing DNA fragment size distribution (~350 bp) following sonication, confirming suitability for library preparation.*

## Enzymatic conversion and library design

Enzymatic conversion and library preparation were performed for samples collected at D−2, D0, 12 hours and D7 for both treatment conditions, using the NEBNext Enzymatic Methyl-seq v2 Kit (NEB-E8015S, New England Biolabs) and the NEBNext LV Unique Dual Index Primer Pairs Set 2A (NEB-E3390S, New England Biolabs), following the manufacturer's protocols. DNA denaturation was carried out using sodium hydroxide. Library amplification was performed by PCR using 5 amplification cycles, as recommended by the protocol for the input amount and expected library complexity.

## Library quantification

Final libraries were assessed and quantified using an Agilent 2100 Bioanalyzer (Agilent Technologies) according to the manufacturer's instructions, to evaluate library size distribution and concentration prior to sequencing (Figure S1). Libraries were then stored at -20 °C and shipped to the sequencing facility for subsequent processing and sequencing.

# 3. Results

## 3.1. DNMTs and TETs are SUMO targets

To investigate whether DNMTs and TETs are directly regulated by SUMOylation at the protein level, we analysed publicly available MS datasets for SUMO modification sites in DNMT and TET family members across different biological systems.

Across multiple studies, both DNMTs and TETs were identified as SUMO targets, although the extent of modification varies substantially depending on the cell type and experimental context (Table 3). In mouse-derived samples, SUMOylation sites were detected for Dnmt1 and Dnmt3a in several studies, with particularly high numbers reported in macrophages (19 sites for Dnmt1) (Goffeney *et al.*, 2025). In contrast, Dnmt3b and Tet proteins showed fewer and more variable SUMO modifications, with Tet3 being the most consistently detected TET family member across datasets. Notably, Tet2 was largely absent from mouse SUMO datasets (Table 3).

Human datasets showed a generally higher number of SUMOylation sites across all family members. For instance, DNMT1, DNMT3A and DNMT3B exhibited extensive SUMOylation, with up to 16 sites detected per protein. Similarly, TET3 displayed a high number of SUMOylation sites (up to 15), suggesting that its SUMOylation may play a conserved regulatory role across species (Table 3).

| Reference | Samples | Dnmt1 | Dnmt3a | Dnmt3b | Tet1 | Tet2 | Tet3 |
|---|---|---|---|---|---|---|---|
| **SUMOylation sites (mouse)** | | | | | | | |
| Hendriks *et al.*, 2018 | Organs from C57BL/6 mice | - | - | - | - | - | 2 |
| Theurillat *et al.*, 2020 | MEF from C57BL/6 mice and mESC | 5 | 5 | 1 | 2 | - | 1 |
| Zhao *et al.*, 2022 | 3T3-L1 preadipocytes | 5 | 2 | - | - | - | 5 |
| Cossec *et al.*, 2023 | Mouse ES-R1 cells | 3 | - | 1 | 6 | - | 1 |
| Goffeney *et al.*, 2025 | RAW 264.7 mouse macrophages | 19 | 3 | - | - | - | 3 |
| **SUMOylation sites (human)** | | | | | | | |
| Hendriks *et al.*, 2017 | HEK | 16 | 7 | 16 | 3 | 7 | 15 |
| Hendriks *et al.*, 2018 | HeLa, U2OS | 11 | 13 | 16 | 11 | 6 | 5 |

***Table 3. SUMOylation sites in DNMT and TET proteins.*** *Summary of identified SUMOylation sites in DNMT and TET family members across mouse and human datasets.*

To further explore the functional relevance of SUMOylation during adipogenesis, we analysed MS data obtained during adipogenic differentiation of 3T3-L1 preadipocytes (Zhao *et al.*, 2022). As shown in Figure 10, the number of SUMOylation sites on Dnmt1, Dnmt3a and Tet3, which are the genes identified as SUMO targets in 3T3-L1 preadipocytes, increased significantly upon adipogenic induction on D0. For Dnmt1, SUMOylation increased significantly from D-2 to D1, followed by a slight decrease at later time points (D3 and D7), although levels remained elevated compared to baseline. Similarly, Dnmt3a exhibited a steady and significant increase in the number of SUMOylated lysins throughout differentiation, indicating a progressive raise in SUMOylation during adipogenesis. The most pronounced changes were observed for Tet3, which showed a strong and highly significant increase in SUMOylation already at D1, remaining elevated at D3 and D7. The magnitude and significance of these changes suggest that Tet3 may be particularly sensitive to SUMO-dependent regulation during adipogenic commitment and that the results in general indicate that SUMOylation dynamically regulates key epigenetic enzymes during adipogenesis.

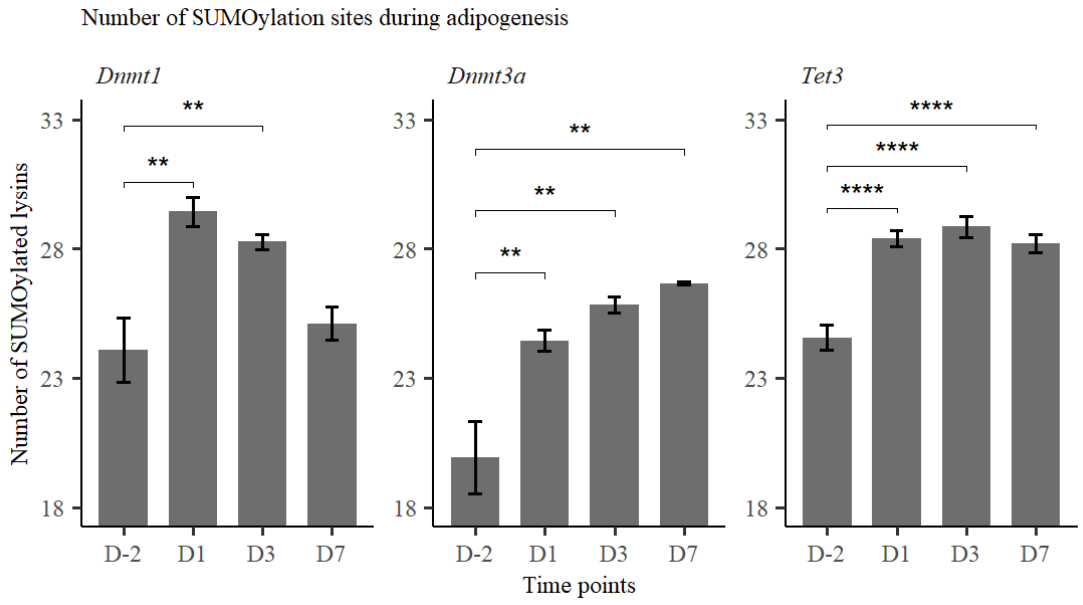


***Figure 10. SUMOylation dynamics of DNMT and TET proteins during adipogenesis.*** *Bar plots showing the total number of SUMOylation sites identified for Dnmt1, Dnmt3a and Tet3 across different stages of adipogenic differentiation (D−2, D1, D3, D7). Data represent variability across four biological replicates. Statistical significance relative to the reference condition (D-2) is indicated by asterisks.*

## 3.2. Transient hypoSUMOylation in adipocyte progenitors enhances adipogenesis

Previously unpublished data from our group suggested that transient inhibition of SUMOylation prior to adipogenic induction enhances adipogenesis, as increased lipid accumulation and upregulation of key adipogenic markers such as *CEBPA* was identified (Nothnagel *et al.*, 2026). To validate these findings, lipid accumulation was assessed during late adipogenesis by ORO staining following a 48-hour treatment with TAK-981 or DMSO prior to adipogenic induction (Figure 11).

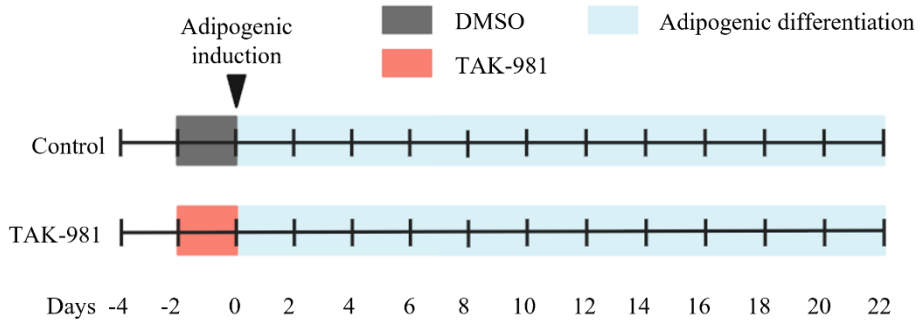


***Figure 11. Experimental design and timeline.*** *Schematic overview of the experimental workflow, including treatment, adipogenic induction and differentiation phase. Created with BioRender.com.*

ORO staining revealed a time-dependent increase in lipid accumulation during adipogenic differentiation, which was consistently enhanced by TAK-981-treated cells (Figure 12A). At D7, only sparse lipid droplets were detectable in control cells, whereas TAK-981-treated cells already exhibited small clusters of ORO-positive cells. Lipid accumulation increased progressively in both conditions. However, TAK-981-treated cultures showed markedly higher staining intensity and abundance at all time points. By D21, treated cells formed dense, confluent clusters of large lipid droplets, while control cultures displayed only limited and weak staining.

To further validate the enhanced adipogenic phenotype, *CEBPA* expression was quantified by RT-qPCR (Figure 12B). In both conditions, *CEBPA* expression increased over the course of differentiation, but this induction was significantly stronger in TAK-981-treated cells, particularly at D3 and D7. At D14, expression levels in treated cells decreased to near control levels.

Together, these results confirm that transient inhibition of SUMOylation prior to adipogenic induction enhances adipogenesis, characterised by increased lipid accumulation and transient overexpression of adipogenic regulators such as *CEBPA*.

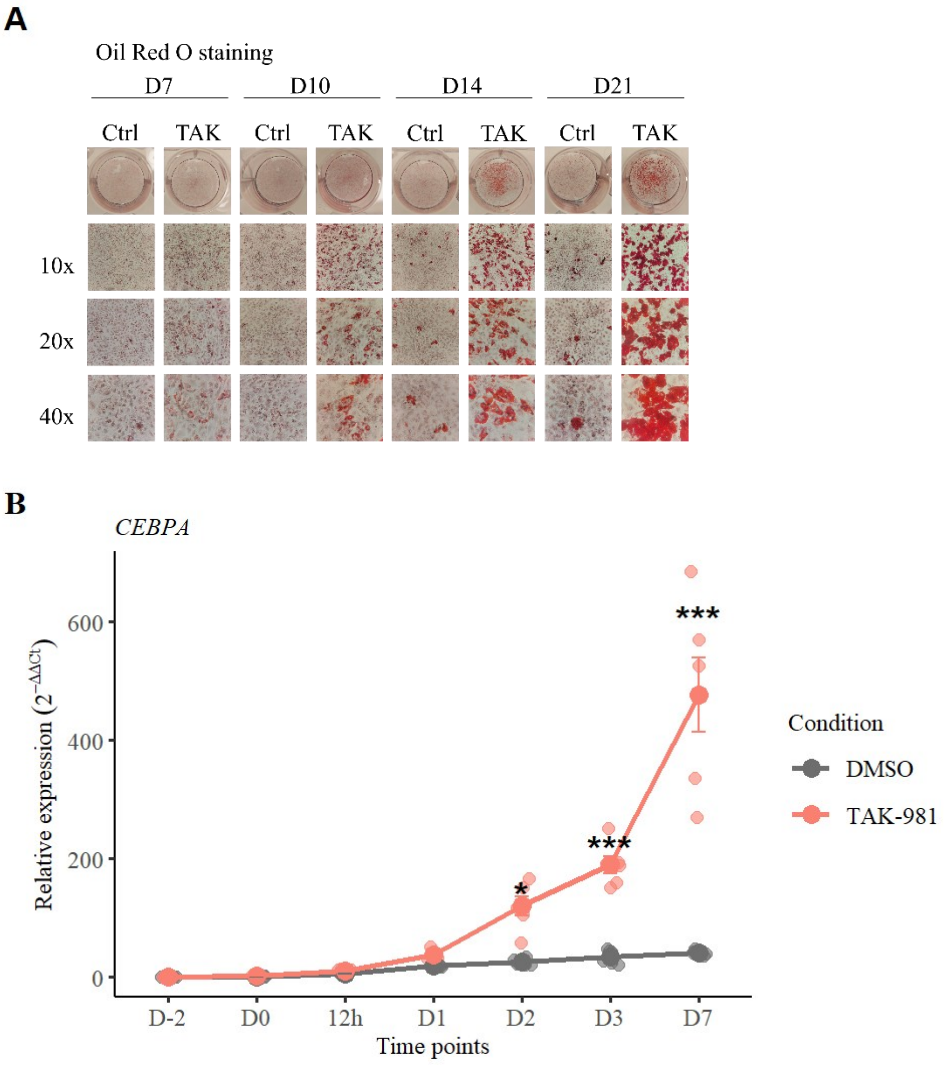


***Figure 12. Enhanced adipogenesis and CEBPA expression following transient TAK-981 treatment.*** *(A) Oil Red O staining showing lipid accumulation during adipogenic differentiation in control (DMSO) and TAK-981-treated cells at days 7, 10, 14 and 21. Representative images are shown at well level and increasing magnifications. (B) Time-course analysis of CEBPA expression measured by RT-qPCR. Expression is shown as $2^{-\Delta\Delta Ct}$ normalised to 18S and day −2. Data represent mean ± variability from 3-9 biological replicates. Outliers were excluded using the IQR method.*

## 3.3. Transient SUMOylation inhibition in adipogenic progenitors perturbs expression of genes involved in DNA methylation in mature adipocytes

Given the stable increase in lipid accumulation and the known role of SUMOylation in epigenetic regulation, we hypothesised that TAK-981 treatment may affect DNA

methylation pathways. To address this, previously generated RNA-seq data from mature adipocytes, collected 21 days after adipogenic induction, (Nothnagel *et al.*, 2026) were analysed with a focus on genes involved in DNA methylation and demethylation.

This analysis revealed a significant upregulation of *TET3* in TAK-981-treated cells, accompanied by a downregulation of *DNMT1* (Figure 13A). In addition, *methyl-CpG-binding protein 2* (*MECP2*) and *ubiquitin-specific-processing protease 7* (*USP7*) were significantly downregulated. Both proteins are known to interact with DNMTs, thereby modulating their enzymatic activity and contributing to the maintenance of DNA methylation patterns (Kunert *et al.*, 2022; Kimura & Shiota, 2023; Felle *et al.*, 2011). Similarly, *M-phase phosphoprotein 8* (*MPHOSPH8*), which has been reported to interact with DNMT3A, also exhibited significant downregulation (Chang *et al.*, 2011).

Interestingly, the observed transcriptional changes were not restricted to factors promoting DNA methylation. Genes involved in active DNA demethylation pathways, including *8-oxoguanine DNA glycosylase 1* (*OGG1*) and *APOBEC3C*, were likewise downregulated. OGG1, a member of the BER glycosylase family, has been shown to facilitate DNA demethylation through its interaction with TET1 (Zhou *et al.*, 2016). The concurrent downregulation of both methylation-promoting and demethylation-associated factors suggests a broader disruption of epigenetic regulatory mechanisms following TAK-981 treatment. Notably, other members of the *DNMT* and *TET* families did not exhibit significant changes in expression under these conditions.

For subsequent experiments, the analysis was narrowed down to the differential expression of the core DNA methylation regulators, particularly the *DNMT* and *TET* gene families. To further assess not only relative expression differences but also absolute expression levels, transcript abundance was visualised in TPM. As shown in Figure 13B, *DNMT1* represents the most highly expressed DNA methyltransferase in mature human adipocytes 21 days after adipogenic induction, whereas *DNMT3B* is only minimally expressed, indicating a limited contribution of de novo methylation activity at this differentiation stage.

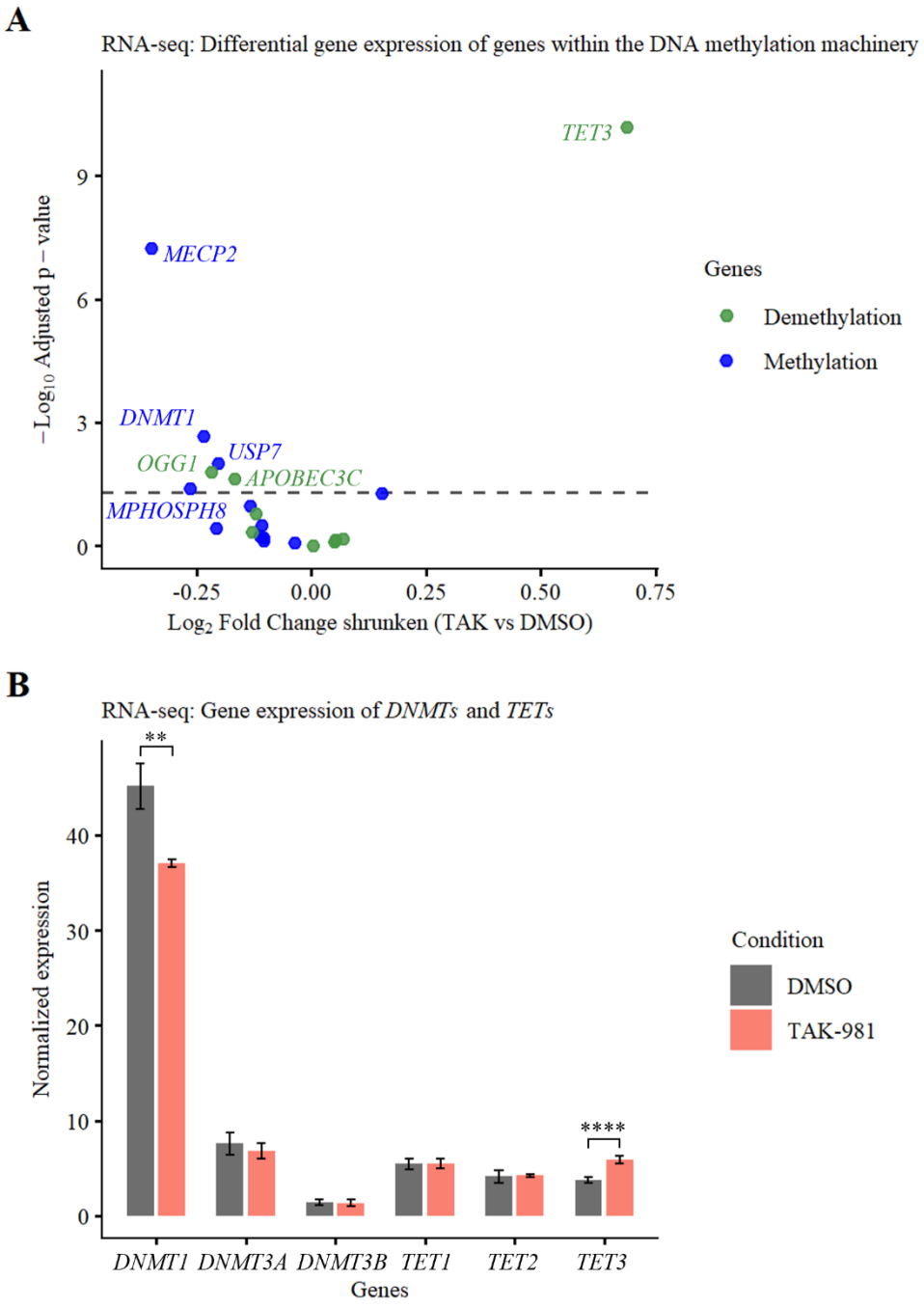


***Figure 13. Differential expression of DNA methylation-related genes following transient hypoSUMOylation.*** *(A) Volcano plot showing differential expression of genes associated with DNA methylation and demethylation 21 days after adipogenic induction. (B) Expression levels (TPM) of DNMT and TET genes in control and TAK-981-treated adipocytes 21 days post induction. Bars represent mean values from three biological replicates.*

Since *DNMTs* and, to a lesser extent, *TETs* are expressed as multiple isoforms (Figure 8), we aimed to determine whether isoform-specific expression changes mirror the overall gene-level differential expression or whether distinct regulatory patterns exist at the isoform level. To address this, we performed an isoform-level analysis based on the raw RNA-seq data.

Overall, none of the investigated isoforms exhibited statistically significant differential expression (Figure 14). However, examining the distribution of effect sizes revealed notable trends. In the case of *DNMT1*, isoforms displayed heterogeneous behaviour, with both positive and negative effect sizes observed. For instance, the non-protein-coding transcript *ENST00000678647.1* showed a tendency toward upregulation, whereas the protein-coding transcript *ENST00000588118.5* appeared to be downregulated. This suggests potential isoform-specific regulation that is not captured at the gene level. For *DNMT3A*, most isoforms showed either mild upregulation or no substantial change, while only a single non-protein-coding transcript (*ENST00000474807.5*) exhibited a trend toward downregulation. In contrast, *DNMT3B* and the *TET* family members (*TET1*, *TET2*, and *TET3*) displayed generally small effect sizes across isoforms, indicating limited variability and no clear directional regulation.

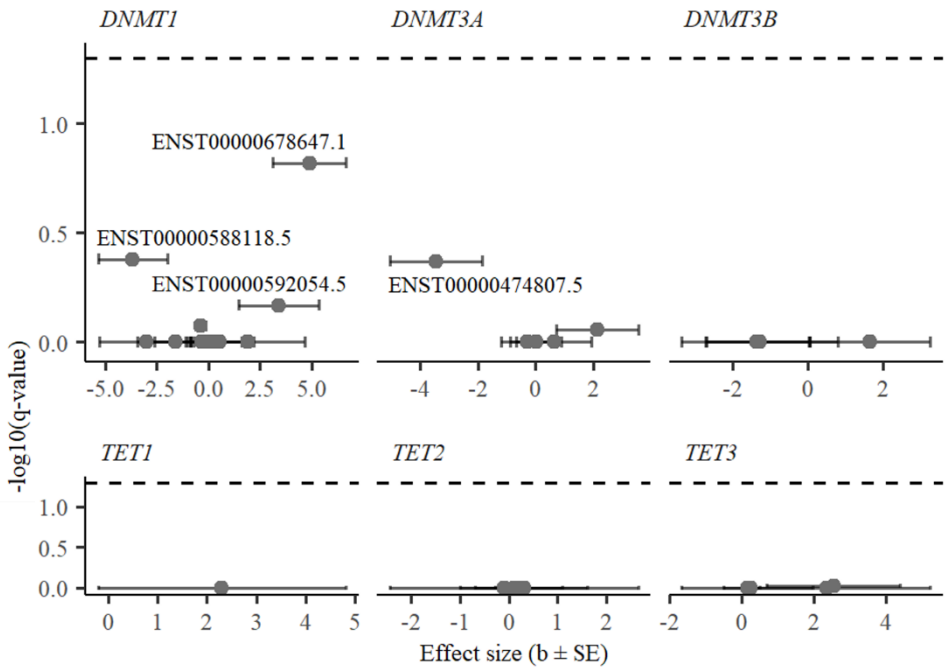


***Figure 14. Isoform-level differential expression of DNMT and TET genes.*** *Volcano plots displaying effect sizes (b ± standard error) versus $-\log_{10}$(q-value) for individual transcript isoforms of DNMT1, DNMT3A, DNMT3B, TET1, TET2 and TET3. Each point represents a single isoform, with horizontal error bars indicating the standard error. The dashed line marks the significance threshold (q = 0.05) and selected isoforms are labelled.*

## 3.4. Immediate effects of transient SUMOylation inhibition in adipogenic progenitors on genes encoding *DNMTs* and *TETs*

Next, we characterised the effect of transient hypoSUMOylation in adipogenic progenitors on *DNMTs* and *TETs* during adipogenesis. The aim was to determine whether genes of the DNA methylation machinery are already differentially expressed during early adipogenesis under TAK-981 compared to DMSO treatment. Early changes in their expression could contribute to epigenetic reprogramming induced by transient SUMOylation inhibition, thereby promoting enhanced differentiation of preadipocytes into mature adipocytes. To address this, the expression of DNMT and TET family members was analysed during adipogenic differentiation under TAK-981 and DMSO control conditions using RT-qPCR, with gene expression assessed at days −2, 0, 0.5, 1, 2, 3, 7, 14 and 21 following adipogenic induction (Figure 11).

*DNMT1* expression did not exhibit significant differential regulation between TAK-981-treated and control cells throughout the first seven days of differentiation (Figure 16). Two primer pairs were used to assess *DNMT1* expression, as they target different RNA species and transcript variants. Primer 1 specifically amplifies pre-mRNA, as it binds to an exon-intron junction. In contrast, primer 2, which binds upstream of primer 1, selectively amplifies mature mRNA by targeting exon-exon junctions (Figure 15). Both primer pairs consistently showed an overall decrease in *DNMT1* transcript levels during early adipogenesis, suggesting a general downregulation of maintenance methylation activity during early differentiation. However, from D7 onwards we see different expression levels between the two primer sets with primer 1 showing significantly upregulation of *DNMT1* in TAK-981-treated cells and *DNMT1* primer 2 showing a slight downregulation in the treatment condition.

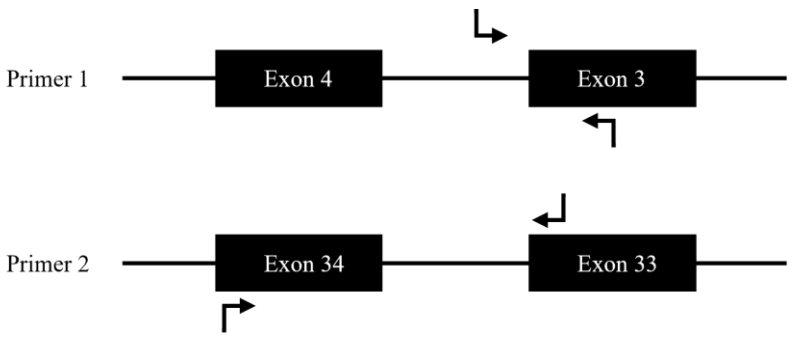


***Figure 15. Schematic representation of the annealing positions of primer 1 and primer 2 within the DNMT1 gene.*** *The primer binding sites are indicated by arrows. Exon numbering corresponds to the reference transcript DNMT1 (ENST00000359526.9).*

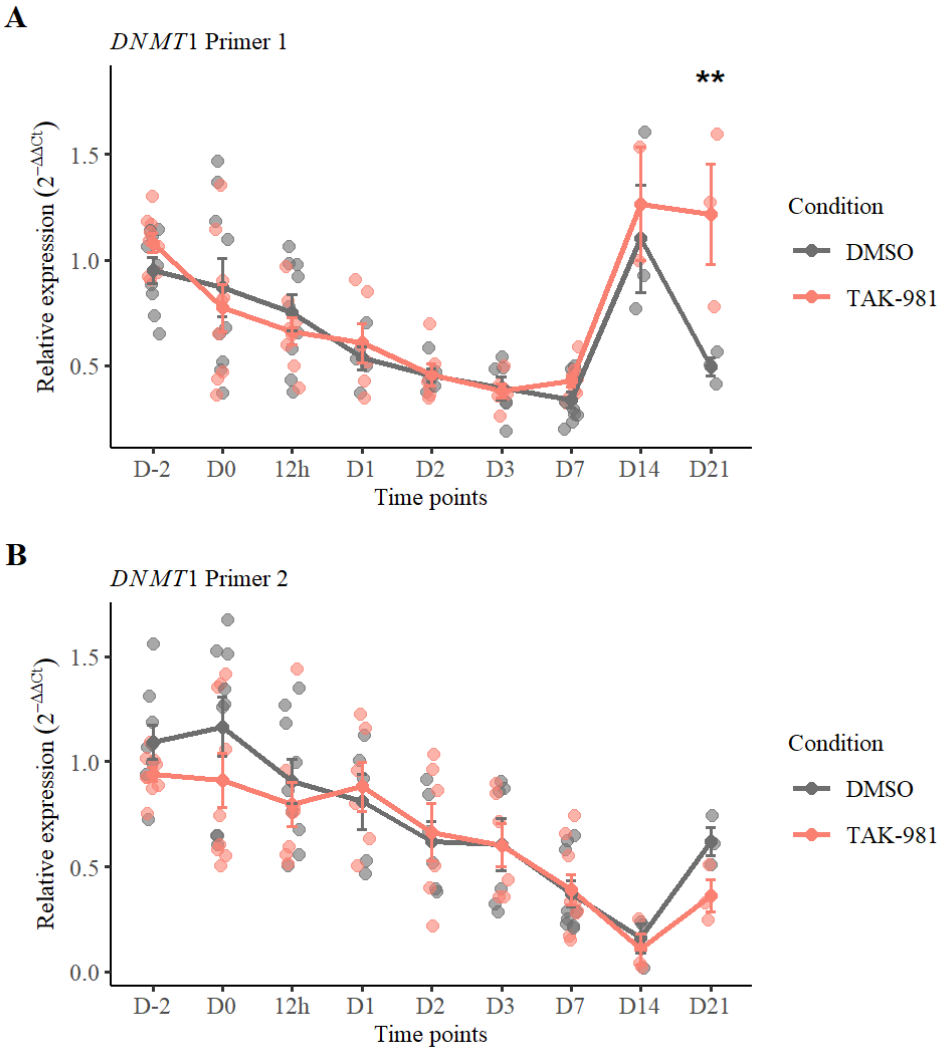


***Figure 16. Time-course analysis of DNMT1 expression.*** *Relative DNMT1 expression measured by RT-qPCR using two primer sets in control and TAK-981-treated cells. Expression values are shown as $2^{-\Delta\Delta Ct}$ normalised to 18S and day −2. Data represent mean ± SEM from 3-9 biological replicates. Outliers were excluded using the IQR method.*

Expression of *DNMT3A* was also analysed using two primer sets that differ in their binding positions, with primer 1 located downstream of primer 2 (Figure 17). *DNMT3A* expression profiles were largely consistent between the two primer sets used, confirming the robustness of the observed expression patterns (Figure 18). In both cases, *DNMT3A* expression followed a similar temporal trajectory in DMSO- and TAK-981-treated cells, characterised by a sharp decline immediately after adipogenic induction, reaching a minimum at 12 hours, followed by a gradual recovery at later time points.

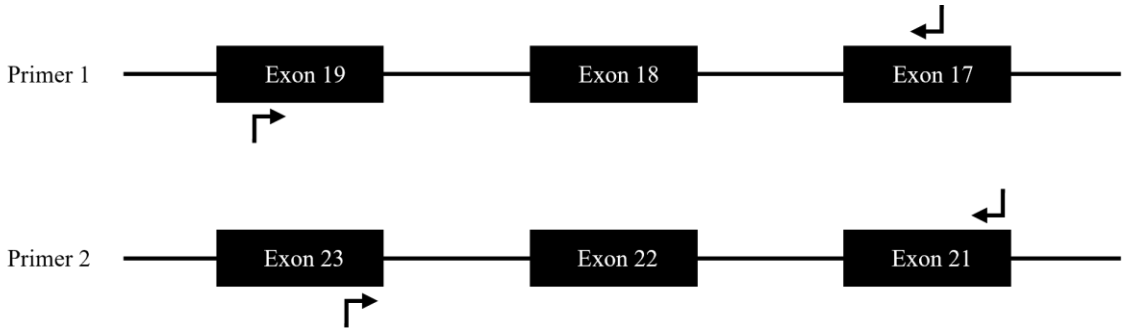


***Figure 17. Schematic representation of the annealing positions of primer 1 and primer 2 within the DNMT3A gene.*** *The primer binding sites are indicated by arrows. Exon numbering corresponds to the reference transcript DNMT3A (ENST00000321117.10).*

Despite this overall similarity, primer 2 (Figure 18B) revealed several statistically significant differences between treatment conditions. Specifically, *DNMT3A* expression was significantly reduced in TAK-981-treated cells at D0 and D3 compared to DMSO controls, indicating a transient downregulation under hypoSUMOylation conditions. This effect appears to be most pronounced during the early phase of differentiation, suggesting that SUMOylation may contribute to the fine-tuning of *DNMT3A* expression during this critical window.

At later stages, particularly at D14 and D21, *DNMT3A* expression increased in both conditions, with significantly higher expression levels in TAK-981-treated cells. Notably, these later time points also showed increased variability, especially in the TAK-981 condition, which may reflect heterogeneous cellular responses during advanced stages of differentiation.

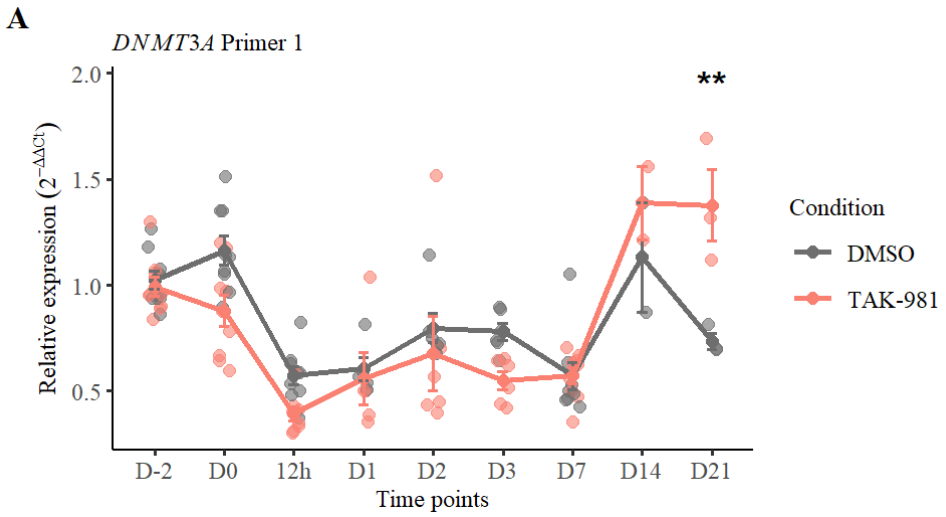

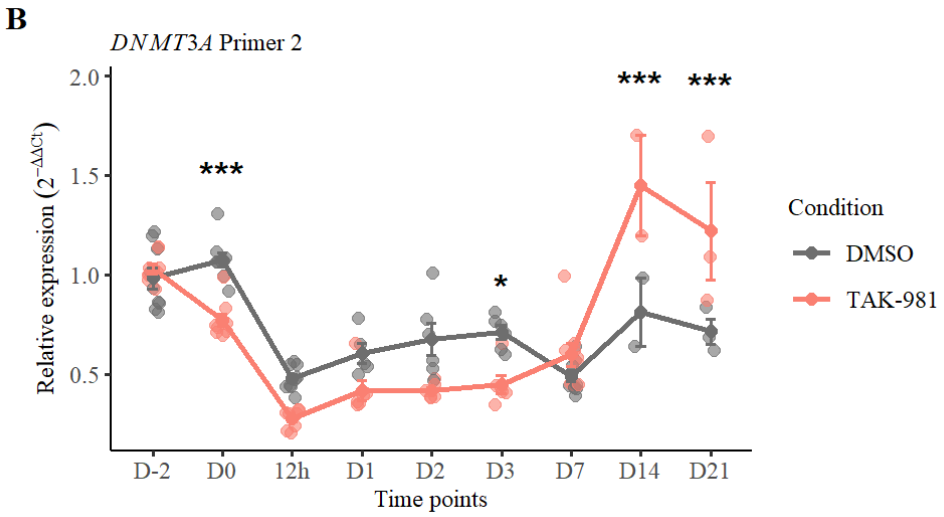


***Figure 18. Time-course analysis of DNMT3A expression.*** *Relative DNMT3A expression measured by RT-qPCR using two primer sets in control and TAK-981-treated cells. Expression values are shown as $2^{-\Delta\Delta Ct}$ normalised to 18S and day −2. Data represent mean ± SEM from 3-9 biological replicates. Outliers were excluded using the IQR method.*

The *de novo* DNA methyltransferase *DNMT3B* showed an expression pattern resembling *DNMT3A* in the DMSO condition, with a peak at D0 followed by a sharp decline after adipogenic induction and a minimal expression value 12 hours post-induction. In contrast to *DNMT3A*, *DNMT3B* did not show significant differential expression between TAK-981-treated and control cells at any time point (Figure 20). The two primer sets used again differ in their binding positions (Figure 19).

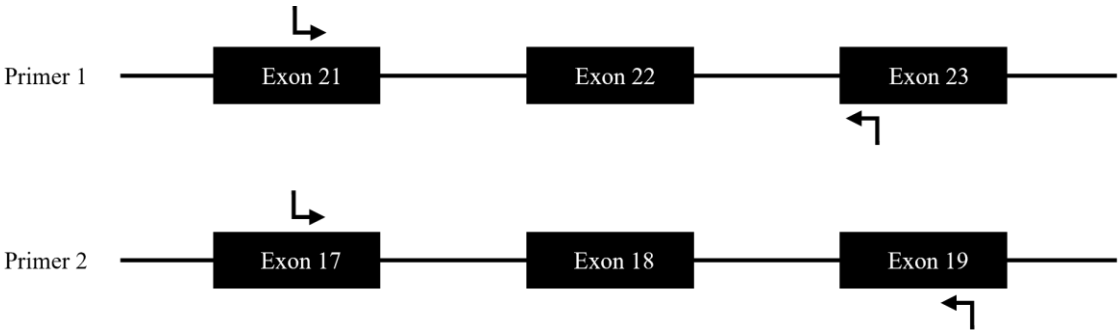


***Figure 19. Schematic representation of the annealing positions of primer 1 and primer 2 within the DNMT3B gene.*** *The primer binding sites are indicated by arrows. Exon numbering corresponds to the reference transcript DNMT3B (ENST00000328111.6).*

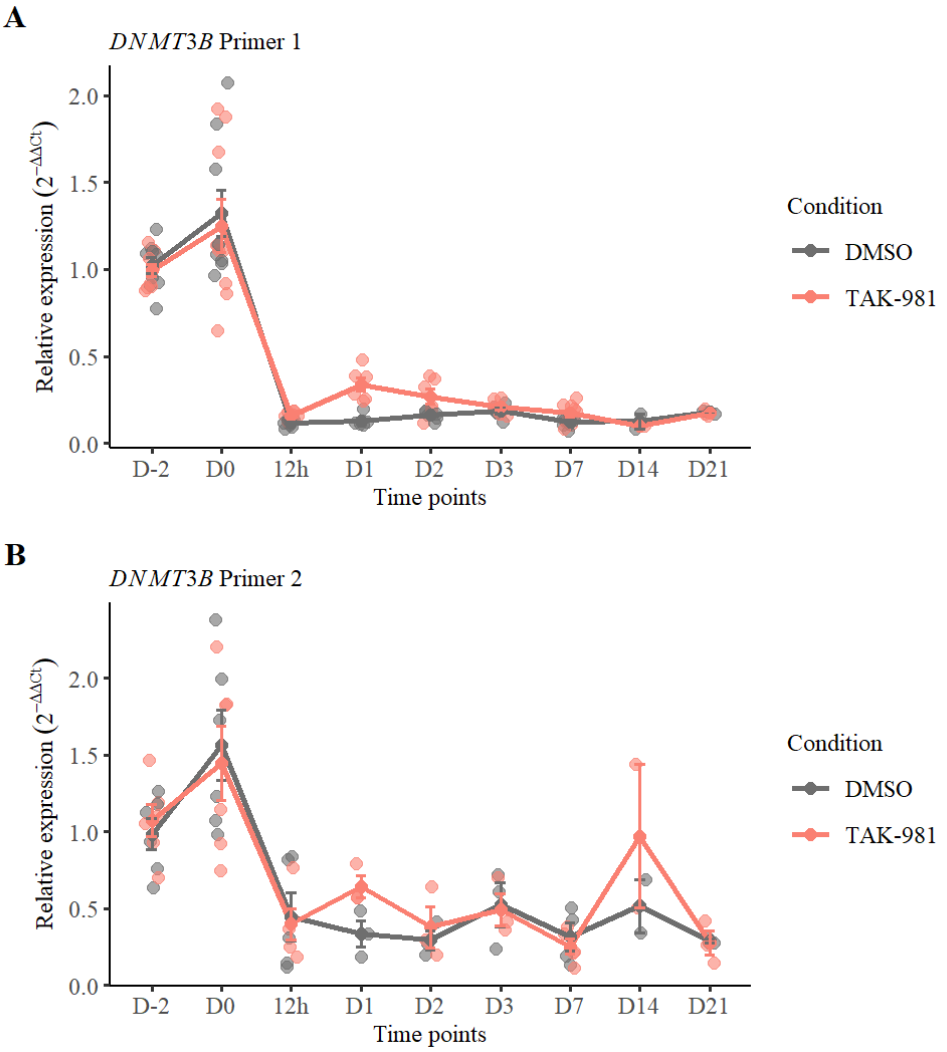


***Figure 20. Time-course analysis of DNMT3B expression.*** *Relative DNMT3B expression measured by RT-qPCR using two primer sets in control and TAK-981-treated cells. Expression values are shown as $2^{-\Delta\Delta Ct}$ normalised to 18S and day −2. Data represent mean ± SEM from 3-9 biological replicates. Outliers were excluded using the IQR method.*

*TET1* expression remained unchanged between conditions until D3. However, starting from D7, a significant upregulation was observed in TAK-981-treated cells, with consistent results across both primer sets. Like *DNMT3A* and *DNMT3B*, *TET1* also exhibited a reduction in expression at 12 hours post-induction in both conditions, suggesting a shared early transcriptional low during adipogenic commitment (Figure 22). The two primer pairs used to assess *TET1* expression target different RNA species and amplification sites. Primer 1 amplifies pre-mRNA, whereas the upstream binding primer 2 specifically amplifies mature mRNA (Figure 21).

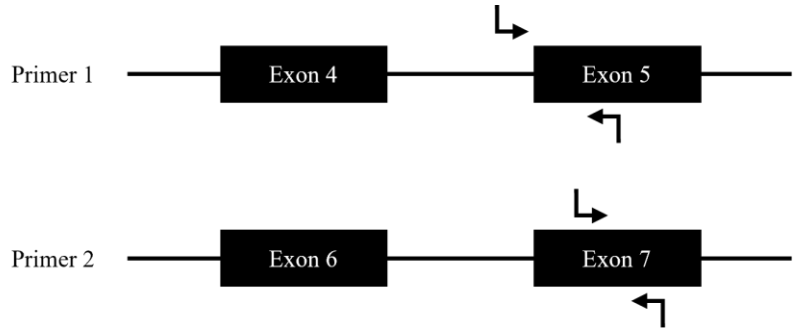


***Figure 21. Schematic representation of the annealing positions of primer 1 and primer 2 within the TET1 gene.*** *The primer binding sites are indicated by arrows. Exon numbering corresponds to the reference transcript TET1 (ENST00000373644.5).*

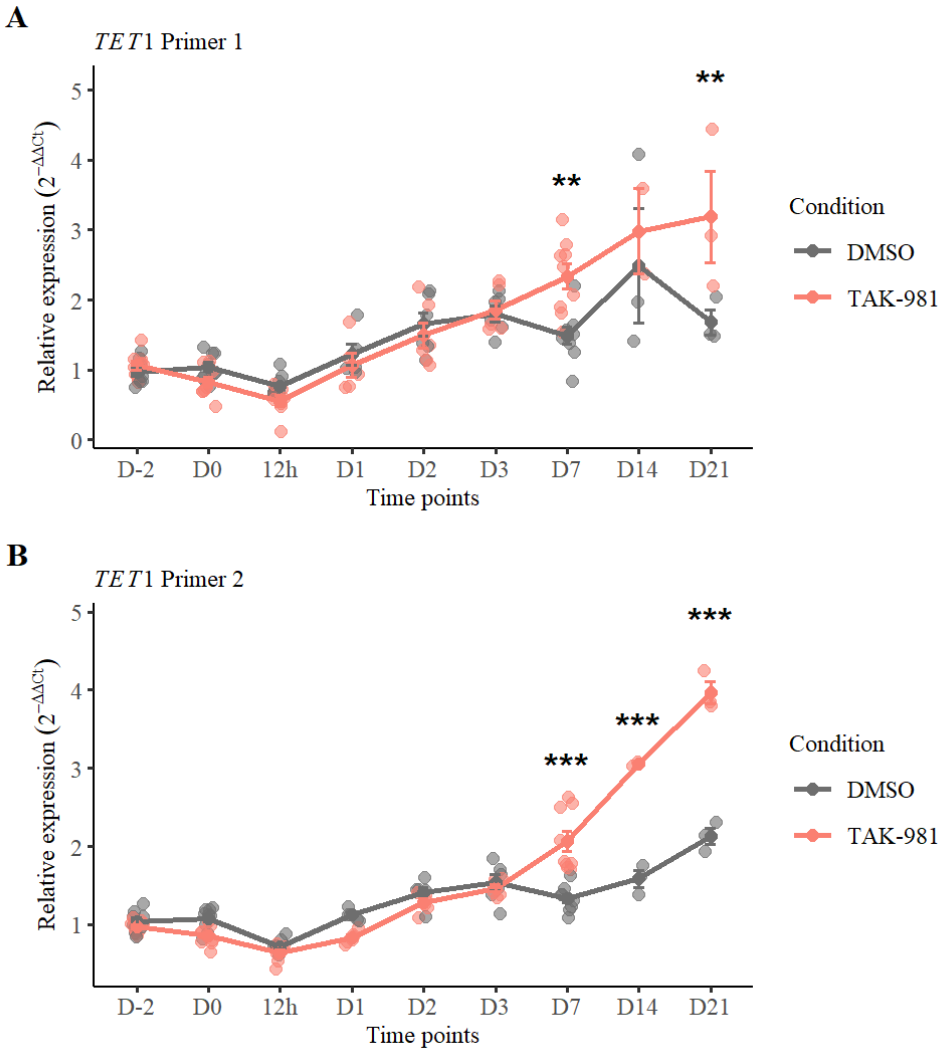


***Figure 22. Time-course analysis of TET1 expression.*** *Relative TET1 expression measured by RT-qPCR using two primer sets in control and TAK-981-treated cells. Expression values are shown as $2^{-\Delta\Delta Ct}$ normalised to 18S and day −2. Data represent mean ± SEM from 3-9 biological replicates. Outliers were excluded using the IQR method.*

Also, for *TET2* expression two different primer sets were used. They target different RNA species and transcript variants, with primer 1 amplifying pre-mRNA and the downstream binding primer 2 amplifying mature mRNA (Figure 23). *TET2* expression patterns differed considerably between the two primer sets and displayed substantial variability across replicates. A statistically significant difference between treatment conditions was only detected with primer set 1, which indicated an upregulation of *TET2* in TAK-981-treated cells. Despite this inconsistency, a general trend toward higher *TET2* expression in TAK-981-treated cells compared to controls was observed from D7 onwards (Figure 24).

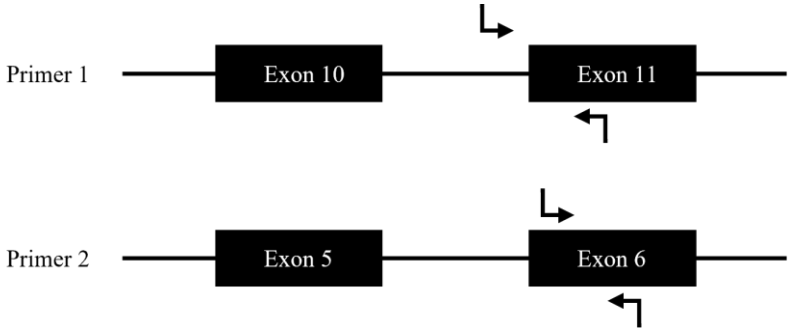


***Figure 23. Schematic representation of the annealing positions of primer 1 and primer 2 within the TET2 gene.*** *The primer binding sites are indicated by arrows. Exon numbering corresponds to the reference transcript TET2 (ENST00000380013.9).*

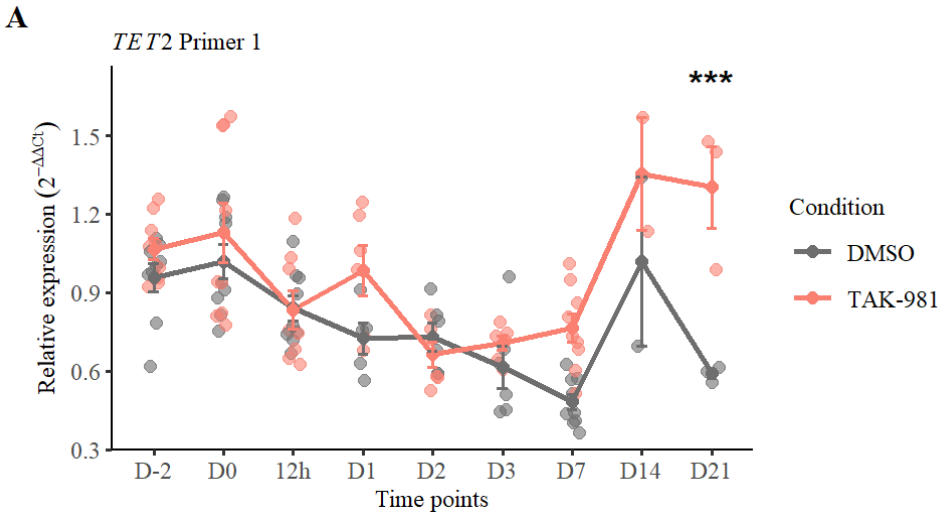

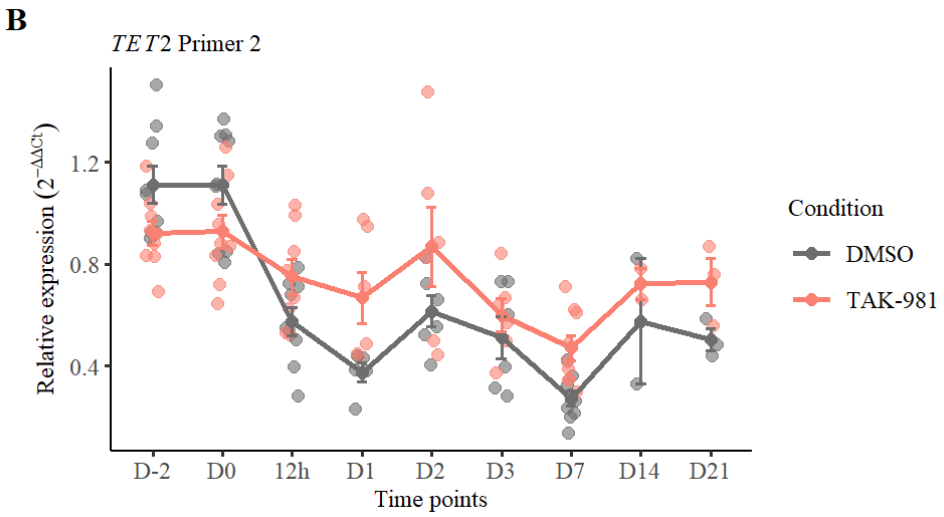


***Figure 24. Time-course analysis of TET2 expression.*** *Relative TET2 expression measured by RT-qPCR using two primer sets in control and TAK-981-treated cells. Expression values are shown as $2^{-\Delta\Delta Ct}$ normalised to 18S and day −2. Data represent mean ± SEM from 3-9 biological replicates. Outliers were excluded using the IQR method.*

For *TET3*, only one primer set, which specifically amplifies mature mRNA, produced a reliable standard curve and was therefore used for further analysis (Figure 25). No significant differences in expression were detected between TAK-981-treated and control cells during the first seven days. However, *TET3* expression was significantly upregulated in the treatment condition at D14 and D21. Notably, a gradual trend toward increased expression in TAK-981-treated cells was already apparent from D2 onwards (Figure 26).


***Figure 25. Schematic representation of the annealing positions of primer 1 within the TET3 gene.*** *The primer binding sites are indicated by arrows. Exon numbering corresponds to the reference transcript TET3 (ENST00000409262.8).*

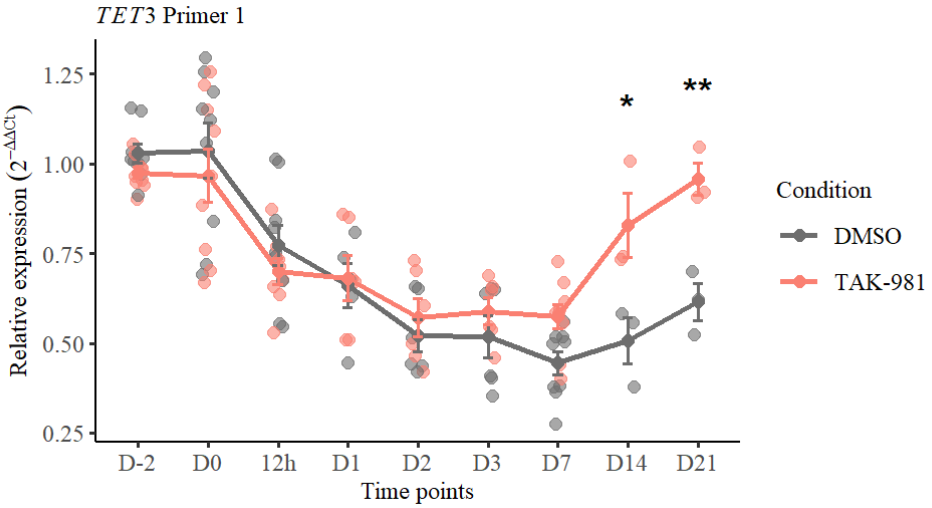


***Figure 26. Time-course analysis of TET3 expression.*** *Relative TET3 expression measured by RT-qPCR using two primer sets in control and TAK-981-treated cells. Expression values are shown as $2^{-\Delta\Delta Ct}$ normalised to 18S and day −2. Data represent mean ± SEM from 3-9 biological replicates. Outliers were excluded using the IQR method.*

## 3.5. Protein expression of DNMTs and TETs following transient SUMOylation inhibition in adipogenic progenitors

To investigate whether differential expression of *DNMT* and *TET* mRNA levels during adipogenesis following transient hypoSUMOylation translate into differential protein expression, protein levels of DNMTs and TETs were examined by Western blot analysis under treatment and control conditions. Protein levels were assessed at days −2, 0, 0.5, 1, 2, 3, 7, 10, 14 and 21 following adipogenic induction (Figure 11).

DNMT1 protein levels were modestly increased in TAK-981-treated cells from D1 to D7 and decreased in D14 and D21 (Figure 27). Overall, a decrease in protein expression during adipogenesis was identified, which is consistent with the gene expression levels (Figure 16). Multiple bands were detected for DNMT1, likely reflecting the presence of different DNMT1 isoforms (Figure 27).

No differences in DNMT3A protein expression were observed between treatment and control conditions during the first ten days following adipogenic induction (Figure 27). At D14 and D21 DNMT3A appeared to be downregulated in TAK-981-treated cells. However, this observation may be a result from unequal protein loading, as indicated by reduced signal intensity in the γ-tubulin loading control at these time points. Consequently, the apparent decrease may not reflect true biological regulation. Instead, DNMT3A levels may be

similarly increased in both conditions, which would be consistent with the observed gene expression data.

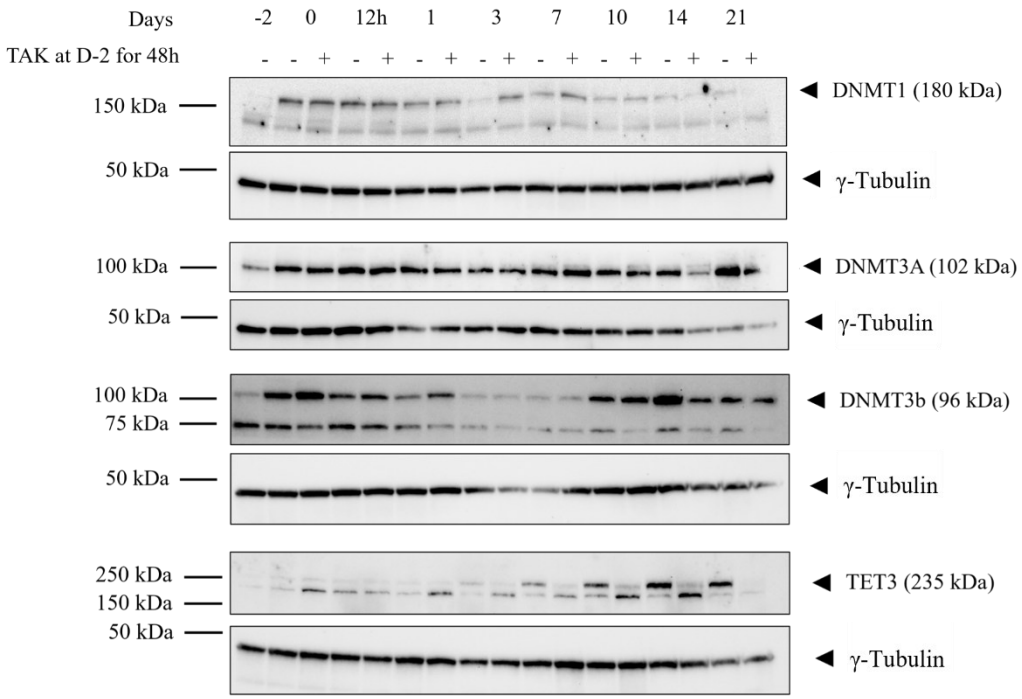


***Figure 27. DNMT and TET protein expression during adipogenesis.*** *Western blot analysis of DNMT1, DNMT3A, DNMT3B and TET3 protein levels in DMSO- and TAK-981-treated cells across the indicated time points. γ-Tubulin served as loading control.*

Western blot analysis of DNMT3B revealed a slight increase in protein expression in TAK-981-treated cells at D1 and a decrease at D14. At all other time points analysed, no notable differences in DNMT3B protein levels were observed between the two conditions (Figure 27). Interestingly, the overall expression patterns up to D7 was largely consistent with the corresponding RT-qPCR results. DNMT3B protein levels increased shortly after treatment and subsequently declined until D7. However, at later time points (D10, D14, and D21), protein levels increased again, a pattern that was not reflected in the RT-qPCR data.

Protein expression of TET1 and TET2 could not be detected under the experimental conditions used. In contrast, Western blot analysis of TET3 revealed two distinct bands at approximately the expected molecular weight. The upper band showed decreased expression in TAK-981-treated cells from D3 onwards, whereas the lower band displayed increased expression in the treatment condition at most time points, except for 12 hours and 21 days post adipogenic induction (Figure 27).

# 4. Discussion

The present study aimed to investigate how transient inhibition of SUMOylation prior to adipogenic induction influences adipocyte differentiation and whether this perturbation affects DNA methylation dynamics through modulation of DNMT and TET expression. By combining transcriptomic analyses, time-resolved gene and protein expression data and global DNA methylation profiling, this work provides new insights into the interplay between SUMOylation and its epigenetic regulation during adipogenesis. Overall, the results indicate that transient SUMOylation inhibition in human adipogenic progenitors is sufficient to induce a stable excess of fat accumulation, which is linked to the overexpression of adipogenic gens like *CEBPA*. Furthermore, transient hypoSUMOylation perturbed the expression of genes and proteins involved in DNA methylation, including DNMTs and TETs. These results suggest that SUMOylation acts as a restrictive regulator of adipogenesis, which might involve epigenetic regulation, such as DNA methylation, via the transcriptional regulation of the expression the DNA methylation machinery components.

## 4.1. Transient hypoSUMOylation enhances adipogenesis

A central finding of this study is that transient inhibition of SUMOylation using TAK-981 prior to adipogenic induction promotes adipocyte differentiation. This is demonstrated by increased lipid accumulation and enhanced expression of the key adipogenic transcription factor *CEBPA*. The observed increase in *CEBPA* expression at early time points (D3 and 7) is particularly interesting. *CEBPA* is a critical regulator of terminal adipocyte differentiation and functions downstream of early transcription factors such as *CEBPB* and *CEBPD* (Siersbæk & Mandrup, 2011; Chang & Kim, 2019). Its transient overexpression suggests that hypoSUMOylation primarily affects early-to-intermediate stages of *CEBPA* expression during adipogenesis. The normalisation of *CEBPA* expression at later stages, despite sustained increases in lipid accumulation, suggests that early transcriptional changes are sufficient to commit cells to a stable enhanced adipogenic trajectory. This is consistent with the idea that adipogenesis is governed by early epigenetic and transcriptional decisions that become self-reinforcing once established (Siersbæk *et al.*, 2017). Thus, transient hypoSUMOylation appears to act as a priming event that shifts the differentiation potential of preadipocytes toward a more adipogenic fate.

In other words, these results are consistent with previous observations from our group (Nothnagel *et al.*, 2026) and align with the concept that SUMOylation functions as a

safeguard of cellular identity, especially stemness (Cossec *et al.*, 2018). By maintaining repressive chromatin environments, SUMOylation prevents inappropriate activation of lineage-specific transcriptional programs, in this case adipogenesis. This has been studied and validated in a recent publication that focussed on histone PTMs rather than DNA methylation as epigenetic regulators of cellular reprogramming (Nothnagel *et al.*, 2026).

## 4.2.SUMOylation could modulate the DNA methylation machinery

RNA-seq analysis revealed that transient hypoSUMOylation prior to adipogenic induction leads to significant changes in the expression of genes involved in DNA methylation and demethylation. Notably, DNMT1 was downregulated, while TET3 was upregulated in mature adipocytes. These findings are in line with a previous study showing that hypoSUMOylation can alter the balance between DNA methylation and demethylation pathways (Cossec *et al.*, 2023). However, the results differ likely due to differences in the model systems, experimental design and the time points analysed. Cossec *et al.* demonstrated that transient inhibition of SUMOylation in mouse embryonic stem cells (mESCs) increases *DNMT3* expression and decreases *TET* expression levels, leading to hypermethylation of pluripotency genes, particularly Nanog. In that study, cells were treated twice with ML-792, a selective inhibitor of the SUMO E1 enzyme, for 48 hours each and expression levels were assessed at the beginning and at the end of each treatment. Consequently, the findings of that study cannot be directly compared to the results of the present RNA-seq analysis, which was performed in mature adipocytes 21 days after adipogenic induction and treatment administration.

DNMT1 is the primary maintenance methyltransferase and plays a key role in preserving DNA methylation patterns during cell division (Lyko, 2017). Its downregulation in mature adipocytes may suggest a reduced capacity to maintain existing methylation marks. However, since human adipogenic progenitors exhibit limited proliferation upon induction, passive DNA demethylation due to impaired maintenance during replication is likely minimal (Li *et al.*, 2021). In contrast, the upregulation of TET3, a key enzyme involved in active DNA demethylation, points toward an increased capacity for removing methylation marks at specific genomic loci. This decrease in DNMT1 and increase in TET3 expression is consistent with the enhanced differentiation towards mature adipocytes observed following transient SUMOylation inhibition. Previous studies in 3T3-L1 cells have shown that DNMT1 expression declines during late adipogenesis and that its depletion at this stage promotes adipocyte maturation (Yang *et al.*, 2016; Gentile *et al.*, 2013). Conversely, TET3

knockdown impairs adipogenesis, highlighting its essential role in this process (Jung *et al.*, 2023; Wu *et al.*, 2025). Consistently, the decrease in DNMT1 and increase in TET3 expression we observed in response to TAK-981 could participate in enhancing adipogenesis following transient SUMOylation inhibition.

However, the simultaneous downregulation of other factors involved in both methylation (e.g. MECP2, USP7, MPHOSPH8) and demethylation (e.g. OGG1, APOBEC3C) suggests that the effects of hypoSUMOylation are not limited to a simple shift toward hypomethylation. Instead, these results indicate a broader disruption of epigenetic homeostasis, as suggested in previous studies, including ours (Nothnagel *et al.*, 2026).

Importantly, the high expression of DNMT1 relative to DNMT3A and DNMT3B in mature adipocytes suggests that maintenance methylation is the dominant mechanism at this stage of differentiation. Therefore, even modest changes in DNMT1 expression or activity could have substantial effects on the epigenetic landscape. This interpretation is supported by previous studies highlighting a central role of DNMT1 in adipogenic differentiation (Yang *et al.*, 2016). However, it is difficult to address this question without having the results of my EM-seq experiment.

## 4.3. Isoform-specific regulation of DNA methylation by SUMOylation

Although gene-level differential expression analysis identified significant changes in *DNMT1* and *TET3*, isoform-level analysis did not reveal statistically significant differences. Nevertheless, trends in effect sizes suggest potential isoform-specific regulation, particularly for *DNMT1*. This observation is interesting, as different isoforms can have distinct regulatory properties, subcellular localisation and functional roles (Kim, 2025; Joshi *et al.*, 2022). The presence of both up- and downregulated *DNMT1* isoforms may explain the apparent discrepancies between RNA-seq and RT-qPCR data, as well as between gene and protein expression levels, given that the primers designed for the RT-qPCR do not capture all transcript variants. To further address this limitation, isoform-specific primers could be designed to enable a direct comparison of isoform expression levels between RT-qPCR and RNA-seq-based isoform analysis.

## 4.4. SUMOylation directly targets DNMTs and TETs

Analysis of publicly available SUMO proteomics datasets provides strong evidence that DNMT and TET proteins are direct targets of SUMOylation. Both mouse and human datasets consistently identified SUMOylation sites on DNMT1, DNMT3A, DNMT3B and TET3, with particularly high numbers observed in human cells. The dynamic increase in SUMOylation of Dnmt1, Dnmt3a and Tet3 during adipogenesis further supports a functional role for SUMOylation in regulating these enzymes. Notably, Tet3 exhibited the most pronounced increase in SUMOylation, suggesting that it may be especially sensitive to SUMO-dependent regulation.

These findings are consistent with previous studies showing that SUMOylation can modulate the activity, stability and chromatin association of epigenetic regulators (Denis *et al.*, 2011). For example, SUMOylation of DNMT1 has been reported to influence their enzymatic activity and interaction with chromatin (Denis *et al.*, 2011; Lee & Muller, 2009; Kroonen *et al.*, 2023). Similarly, SUMOylation of TET3 protein may affect its stability and its catalytic efficiency (Liu *et al.* 2023). Taken together, this suggests that SUMOylation regulates DNA methylation machinery at multiple levels, including transcription and protein modification. To further investigate the functional impact of SUMOylation on DNA methylation enzymes, future experiments could assess the SUMOylation status of DNMTs and TETs using immunoprecipitation-based approaches. In addition, genome-wide DNA methylation profiling will be performed to determine whether changes in SUMOylation affect global or locus-specific DNA methylation levels, thereby providing functional insight into altered DNMT and TET activity.

## 4.5. Temporal dynamics of DNMT and TET gene and protein expression

Time-resolved RT-qPCR and Western blot analysis revealed that DNMT and TET gene and protein expression is dynamically regulated during adipogenesis and that these dynamics are modulated by hypoSUMOylation in a stage-specific manner.

For DNMT1, both gene and protein expression decreased during early adipogenesis, consistent with previous reports (Yang *et al.*, 2016; Gentile *et al.*, 2013). This decline likely reflects the reduced need for maintenance methylation as cells exit the cell cycle and commit to differentiation. The modest increase in DNMT1 protein levels in TAK-981-treated cells at D3 and D7 may indicate a compensatory response due to altered protein stability under

hypoSUMOylation conditions. Inhibition of SUMOylation did not alter *DNMT1* expression within the first seven days after adipogenic induction, suggesting that SUMOylation does not affect *DNMT1* transcript levels during early differentiation. From D7 onwards, however, divergent *DNMT1* expression patterns were observed between the two primer sets. These discrepancies may arise from differences in the amplified regions, potentially capturing distinct transcript variants. This interpretation is supported by the isoform analysis, which revealed heterogeneous expression patterns among *DNMT1* transcripts in mature adipocytes. In addition, primer 1 specifically amplifies pre-mRNA, which may further contribute to the observed differences between primer sets. The DNMT1 protein expression during late adipogenesis was slightly decreased in TAK-981-treated cells at D14 and D21, which is consistent with the lower gene expression in the RNA-seq data.

*DNMT3A* exhibited a transient downregulation in TAK-981-treated cells during early differentiation, followed by increased expression at later stages (D14 and D21). It has been shown that *DNMT3A* overexpression stimulates proliferation while suppressing adipogenic differentiation (Wu *et al.*, 2025). Thus, the transient reduction of *DNMT3A* during early adipogenesis observed under hypoSUMOylation may relieve this inhibitory constraint, thereby facilitating adipogenic commitment. The subsequent increase in *DNMT3A* expression at later stages may then support adipocyte maturation, consistent with its reported upregulation during late adipogenesis (Yang *et al.*, 2016). Together, these findings suggest that temporal modulation of *DNMT3A* is critical for proper adipogenic differentiation and may contribute to the enhanced adipogenesis observed under transient SUMOylation inhibition.

In contrast, DNMT3B gene and protein expression showed minimal changes between conditions, consistent with its low expression in adipocytes and potentially limited role in adipogenesis (Yang *et al.*, 2016). The early transcriptional valley observed across multiple genes at 12 hours post-induction may reflect a global transcriptional reorganisation during adipogenic commitment.

Among the TET enzymes, particularly *TET1* and *TET3* showed increased expression at later stages in TAK-981-treated cells, while *TET2* exhibited variable and less consistent results. The upregulation of *TET* genes during late differentiation suggests an enhanced DNA demethylation capacity, which may facilitate the activation of adipocyte-specific gene expression programs. This is in line with previous studies demonstrating that TET-mediated

hydroxymethylation promotes transcriptional activation of key adipogenic regulators (Qian *et al.*, 2021, Liu *et al.*, 2023, Jung *et al.*, 2023, Wu *et al.*, 2025).

At the protein level, the transcriptional patterns of TET enzymes were only partially confirmed. TET1 and TET2 proteins were not detectable under the experimental conditions used, likely due to low protein abundance, technical limitations of the antibodies or suboptimal experimental conditions. In contrast, TET3 protein was readily detectable and exhibited a more complex expression pattern. Two distinct bands were observed, likely representing different isoforms or post-translationally modified forms of TET3. Notably, in TAK-981-treated cells, the upper band showed decreased expression from D3 onwards, whereas the lower band showed increased expression at most time points, except at 12 hours and D21. This divergence between the two TET3 bands suggests isoform- or modification-specific regulation of TET3 in response to SUMOylation inhibition.

Three protein-coding isoforms of *TET3* are generated by alternative promoter usage and splicing (Joshi *et al.*, 2022). In humans, both full-length TET3 and a shorter isoform (TET3s) have been described. The short isoform lacks a DNA-binding domain and relies on interactions with other DNA-binding proteins, leading to context-dependent and sometimes opposing functions compared to full-length TET3. These properties could explain the differential band intensities observed and support the idea that the two bands correspond to distinct functional isoforms. Given that different TET isoforms vary in genomic targeting and regulatory activity (Joshi *et al.*, 2022), this isoform-specific modulation could have important consequences for locus-specific DNA demethylation during adipogenesis. The increase in the lower TET3 band in TAK-981-treated cells coincides with enhanced adipogenesis, suggesting that this specific form of TET3 is functionally linked to adipogenic gene activation. These findings indicate that SUMOylation may regulate not only the expression but also the functional composition of TET3 protein, thereby fine-tuning DNA demethylation dynamics during adipocyte differentiation.

Overall, TET3 emerges as a robust target of interest in the context of SUMOylation-dependent epigenetic regulation, as its gene expression is consistently upregulated under TAK-981 treatment and corresponding changes in TET3 protein levels are also observed between conditions. Consequently, transient inhibition of SUMOylation could enhance DNA demethylation at adipogenic genes and enhancers, thereby promoting their transcriptional activation and contributing to the observed hyperadipogenic phenotype. Together, this suggests that SUMOylation may indirectly repress DNA demethylation by dampening TET3

expression. However, in the absence of the results of the EM-seq analysis, it remains unclear whether these changes in TET3 are causally linked to the altered expression of adipogenic programs. Nevertheless, existing literature supports a role for TET enzymes in regulating adipogenic gene expression, further strengthening the hypothesis that TET3 may act as a key mediator in this process (Qian *et al.*, 2021, Liu *et al.*, 2023, Jung *et al.*, 2023, Wu *et al.*, 2025).

## 4.6. Limitations and future perspectives

Despite providing insights into the regulation of the DNA methylation machinery under transient hypoSUMOylation prior to adipogenic induction, several limitations should be considered.

First, many of the observed effects were not consistent between the transcriptional and protein levels and, in some cases, even appeared contradictory. These discrepancies may arise from multiple factors, including post-transcriptional regulation, differences in protein stability and technical variability in Western blot analysis. However, the underlying mechanisms were not further investigated. Since, SUMOylation is known to affect protein stability, subcellular localisation and protein-protein interactions, the observed differences between mRNA and protein expression may also reflect altered protein turnover or SUMO-dependent stabilisation (Chymkowitch *et al.*, 2015; Paakinaho *et al.*, 2021). Nevertheless, without experimental validation, these interpretations remain speculative. Such validation could include protein half-life measurements (e.g. cycloheximide chase assays), assessment of protein stability under proteasome inhibition and analysis of subcellular localisation by immunofluorescence. In addition, immunoprecipitation-based approaches could be used to confirm SUMOylation of the target proteins.

Second, the detection of multiple DNMT1 and TET3 protein bands complicates data interpretation. These bands may represent alternative isoforms (Jin *et al.*, 2016; Saini *et al.*, 2017) or post-translationally modified forms, including SUMOylated or ubiquitinated species (Denis *et al.*, 2011; Joshi *et al.*, 2022). In combination with the isoform analysis, which revealed differences in effects sizes between transcript variants, particularly for DNMT1, it is plausible that the bands correspond to distinct isoforms. However, based on the Western blot results, a more pronounced isoform-specific effect would have been expected for TET3. The differential regulation of these bands upon TAK-981 treatment further highlights the complexity of SUMO-dependent protein regulation. Given the known

diversity of TET3 isoforms and their distinct and, in some cases, even opposing functions due to differences in their ability to bind specific regulatory regions (Joshi *et al.*, 2022), future studies should aim to systematically characterise isoform-specific expression and function during adipogenesis under altered SUMOylation conditions.

Third, the inability to detect TET1 and TET2 protein expression represents a technical limitation. This may be due to low endogenous protein abundance in adipocytes, limited antibody sensitivity or suboptimal experimental conditions. As a result, conclusions regarding the role of TET1 and TET2 are restricted to transcriptional data and remain incomplete. Future work should therefore include optimisation of protein detection methods, such as testing alternative antibodies and increasing protein input.

Finally, although expression changes of DNA methylation regulators were characterised, their functional consequences on global or locus-specific DNA methylation remain unresolved, as the analysis of the EM-seq data is still ongoing (as of March 2026). Without direct quantification of 5-methylcytosine or 5-hydroxymethylcytosine levels, it remains unclear whether the observed molecular changes translate into altered DNA methylation patterns at adipogenic gene loci or across the genome.

# 5. Conclusion

In summary, this study indicates that transient inhibition of SUMOylation prior to adipogenic induction enhances adipogenesis and adipogenic transcription and modulates the expression of key components of the DNA methylation machinery in a temporally controlled manner. The data support the idea that SUMOylation restricts adipogenic differentiation by maintaining epigenetic stability, whereas its inhibition promotes a more permissive chromatin state through coordinated changes in DNMT and TET expression and potentially their activity.

The results show that transient hypoSUMOylation prior to adipogenesis reduces DNMT1 gene and protein expression and increases *TET* expression, most notable *TET3*, in the late stage of differentiation. Together, these dynamics may contribute to the establishment of a more open chromatin environment that facilitates the activation of adipogenic gene programs. Although performed, the assessment of global DNA methylation by EM-seq is still missing from this study, due to time constrains, which for the moment prevents the validation of this hypothesis, though it is supported by the literature.

Overall, these findings provide new insights into the crosstalk between SUMOylation and epigenetic regulation and highlight the importance of SUMOylation in controlling cell fate decisions. Given the central role of adipose tissue in metabolic health, a better understanding of these mechanisms may have important implications for the development of novel therapeutic strategies for obesity and related metabolic diseases.

# 6. References


Abdalla, B. A. *et al.* A novel Dnmt3a1 transcript inhibits adipogenesis. *Front. Physiol.* **9**, 1270 (2018).

Ashburner, M. *et al.* Gene ontology: tool for the unification of biology. The Gene Ontology Consortium. *Nat. Genet.* **25**, 25-29 (2000).

Baig, M. S. *et al.* Dynamic sumoylation of promoter-bound general transcription factors facilitates transcription by RNA polymerase II. *PLoS Genet.* **17**, e1009828 (2021).

Bhutani, N., Burns, D. M. & Blau, H. M. DNA demethylation dynamics. *Cell* **146**, 866-872 (2011).

Bjune, J.-I. *et al.* IRX3 controls a SUMOylation-dependent differentiation switch in adipocyte precursor cells. *Nat. Commun.* **16**, 7248 (2025).

Carbon, S. *et al.* AmiGO: online access to ontology and annotation data. *Bioinformatics* **25**, 288-289 (2009).

Catalán, V. *et al.* Validation of endogenous control genes in human adipose tissue: relevance to obesity and obesity-associated type 2 diabetes mellitus. *Horm. Metab. Res.* **39**, 495-500 (2007).

Chait, A. & den Hartigh, L. J. Adipose tissue distribution, inflammation and its metabolic consequences, including diabetes and cardiovascular disease. *Front. Cardiovasc. Med.* **7**, 22 (2020).

Chang, E. & Kim, C. Y. Natural products and obesity: A focus on the regulation of mitotic clonal expansion during adipogenesis. *Molecules* **24**, E1157 (2019).

Chang, Y. *et al.* MPP8 mediates the interactions between DNA methyltransferase Dnmt3a and H3K9 methyltransferase GLP/G9a. *Nat. Commun.* **2**, 533 (2011).

Chung, S. S. *et al.* Control of adipogenesis by the SUMO-specific protease SENP2. *Mol. Cell. Biol.* **30**, 2135-2146 (2010).

Chymkowitch, P., Nguéa P, A. & Enserink, J. M. SUMO-regulated transcription: challenging the dogma. *Bioessays* **37**, 1095-1105 (2015).

Cierzniak, A. *et al.* DNA methylation in adipocytes from visceral and subcutaneous adipose tissue influences insulin-signaling gene expression in obese individuals. *Int. J. Obes. (Lond)* **45**, 650-658 (2021).

Cignarelli, A. Role of UBC9 in adipogenesis. *Endocrinology* **151**, 5255-5266 (2010).

Claussnitzer, M. *et al.* FTO obesity variant circuitry and adipocyte browning in humans. *N. Engl. J. Med.* **373**, 895-907 (2015).

Cossec, J.-C. SUMO safeguards cell identities by enforcing transcriptional programs. *Cell Stem Cell* **23**, 742-757 (2018).

Cossec, J.-C. *et al.* Transient suppression of SUMOylation in embryonic stem cells generates embryo-like structures. *Cell Rep.* **42**, 112380 (2023).

Cox, A. R. Ube2i deletion in adipose tissue causes lipoatrophy. *Mol Metab* **48**, (2021).

Demarque, M. D. Sumoylation by Ubc9 regulates intestinal stem cell renewal. *Gastroenterology* **140**, 286-296 (2011).

Denis, H., Ndlovu, M. N. & Fuks, F. Regulation of mammalian DNA methyltransferases: a route to new mechanisms. *EMBO Rep.* **12**, 647-656 (2011).

Du, J., Zhao, L., Kang, Q., He, Y. & Bi, Y. An optimized method for Oil Red O staining with the salicylic acid ethanol solution. *Adipocyte* **12**, 2179334 (2023).

Dudek, A. Z. *et al.* Phase 1/2 study of the novel SUMOylation inhibitor TAK-981 in adult patients (pts) with advanced or metastatic solid tumors or relapsed/refractory (RR) hematologic malignancies. *J. Clin. Oncol.* **39**, TPS2667-TPS2667 (2021).

Durcin, M. *et al.* Characterisation of adipocyte-derived extracellular vesicle subtypes identifies distinct protein and lipid signatures for large and small extracellular vesicles. *J. Extracell. Vesicles* **6**, 1305677 (2017).

Emont, M. P. *et al.* A single-cell atlas of human and mouse white adipose tissue. *Nature* **603**, 926-933 (2022).

Ewels, P. A. *et al.* The nf-core framework for community-curated bioinformatics pipelines. *Nat. Biotechnol.* **38**, 276-278 (2020).

Felle, M. *et al.* The USP7/Dnmt1 complex stimulates the DNA methylation activity of Dnmt1 and regulates the stability of UHRF1. *Nucleic Acids Res.* **39**, 8355-8365 (2011).

Finucane, H. K. *et al.* Partitioning heritability by functional annotation using genome-wide association summary statistics. *Nat. Genet.* **47**, 1228-1235 (2015).

Garvin, A. J. *et al.* The deSUMOylase SENP7 promotes chromatin relaxation for homologous recombination DNA repair. *EMBO Rep.* **14**, 975-983 (2013).

Londoño Gentile, T. *et al.* DNMT1 is regulated by ATP-citrate lyase and maintains methylation patterns during adipocyte differentiation. *Mol. Cell. Biol.* **33**, 3864-3878 (2013).

Goffeney, A. *et al.* SUMO operates from a unique long tandem repeat to keep innate immunity in check. *Nucleic Acids Res.* **53**, gkaf750 (2025).

Gómez-Hernández, A., Beneit, N., Díaz-Castroverde, S. & Escribano, Ó. Differential role of adipose tissues in obesity and related metabolic and vascular complications. *Int. J. Endocrinol.* **2016**, 1216783 (2016).

Harvey, I. Adipose tissue in health and disease. *Open Biol* **10**, (2020).

Hegde, M. & Joshi, M. B. Regulation of DNMT isoforms in breast tumors. *J Cancer Res Clin Oncol* **147**, 937-971 (2021).

Hendriks, I. A. *et al.* Site-specific characterization of endogenous SUMOylation across species and organs. *Nat. Commun.* **9**, 2456 (2018).

Hendriks, I. A. *et al.* Site-specific mapping of the human SUMO proteome reveals co-modification with phosphorylation. *Nat. Struct. Mol. Biol.* **24**, 325-336 (2017).

Herbers, E. *et al.* Preventing white adipocyte browning during differentiation in vitro: The effect of differentiation protocols on metabolic and mitochondrial phenotypes. *Stem Cells Int.* **2022**, 3308194 (2022).

Jamal, A. BTYNB, an inhibitor of RNA binding protein IGF2BP1, reduces proliferation and induces differentiation of leukemic cancer cells. *Saudi J Biol Sci* **30**, (2023).

Jin, S.-G. *et al.* Tet3 reads 5-carboxylcytosine through its CXXC domain and is a potential guardian against neurodegeneration. *Cell Rep.* **14**, 493-505 (2016).

Joshi, K., Liu, S., Breslin S J, P. & Zhang, J. Mechanisms that regulate the activities of TET proteins. *Cell. Mol. Life Sci.* **79**, 363 (2022).

Jung, B. C. *et al.* TET3 plays a critical role in white adipose development and diet-induced remodeling. *Cell Rep.* **42**, 113196 (2023).

Kalligeros, M. Association of obesity with disease severity among patients with COVID-19. *Obesity* **28**, 1200-1204 (2020).

Kent, W. J. The Human Genome Browser at UCSC. *Genome Res.* **12**, 996-1006 (2002).

Kim, D. J. The role of the DNA methyltransferase family and the therapeutic potential of DNMT inhibitors in tumor treatment. *Curr. Oncol.* **32**, 88 (2025).

Kimura, H. & Shiota, K. Methyl-CpG-binding protein, MeCP2, is a target molecule for maintenance DNA methyltransferase, Dnmt1. *J. Biol. Chem.* **278**, 4806-4812 (2003).

Kitahara, C. M. *et al.* Association between class III obesity (BMI of 40-59 kg/m2) and mortality: a pooled analysis of 20 prospective studies. *PLoS Med.* **11**, e1001673 (2014).

Kroonen, J. S. *et al.* Inhibition of SUMOylation enhances DNA hypomethylating drug efficacy to reduce outgrowth of hematopoietic malignancies. *Leukemia* **37**, 864-876 (2023).

Kunert, S. *et al.* The MECP2-TRD domain interacts with the DNMT3A-ADD domain at the H3-tail binding site. *Protein Sci.* **32**, e4542 (2023).

Lee, B. & Muller, M. T. SUMOylation enhances DNA methyltransferase 1 activity. *Biochem. J.* **421**, 449-461 (2009).

Lefterova, M. I., Haakonsson, A. K., Lazar, M. A. & Mandrup, S. PPARγ and the global map of adipogenesis and beyond. *Trends Endocrinol. Metab.* **25**, 293-302 (2014).

Li, Q. *et al.* Obesity and hyperinsulinemia drive adipocytes to activate a cell cycle program and senesce. *Nat. Med.* **27**, 1941-1953 (2021).

Liao, J. *et al.* Targeted disruption of DNMT1, DNMT3A and DNMT3B in human embryonic stem cells. *Nat. Genet.* **47**, 469-478 (2015).

Ling, Y. *et al.* Modification of de novo DNA methyltransferase 3a (Dnmt3a) by SUMO-1 modulates its interaction with histone deacetylases (HDACs) and its capacity to repress transcription. *Nucleic Acids Res.* **32**, 598-610 (2004).

Linhart, H. G. C/EBPα is required for differentiation of white, but not brown, adipose tissue. *Proc Natl Acad Sci* **98**, 12532-12537 (2001).

Liu, B. SENP1 controls adipocyte differentiation. *J Biol Chem* **289**, 22358-22364 (2014).

Liu, F. *et al.* SUMO1 modification stabilizes TET3 protein and increases colorectal cancer radiation therapy sensitivity. *Int. J. Radiat. Oncol. Biol. Phys.* **117**, 942-954 (2023).

Liu, Y. *et al.* TET2 is recruited by CREB to promote Cebpb, Cebpa, and Pparg transcription by facilitating hydroxymethylation during adipocyte differentiation. *iScience* **26**, 108312 (2023).

Livak, K. J. & Schmittgen, T. D. Analysis of relative gene expression data using real-time quantitative PCR and the 2(-Delta Delta C(T)) Method. *Methods* **25**, 402-408 (2001).

Locke, A. E. *et al.* Genetic studies of body mass index yield new insights for obesity biology. *Nature* **518**, 197-206 (2015).

Loos, R. J. F. & Yeo, G. S. H. The genetics of obesity: from discovery to biology. *Nat. Rev. Genet.* **23**, 120-133 (2022).

Lyko, F. The DNA methyltransferase family: a versatile toolkit for epigenetic regulation. *Nat. Rev. Genet.* **19**, 81-92 (2018).

Maurano, M. T. *et al.* Systematic localization of common disease-associated variation in regulatory DNA. *Science* **337**, 1190-1195 (2012).

Mikkonen, L., Hirvonen, J. & Jänne, O. A. SUMO-1 regulates body weight and adipogenesis via PPARγ in male and female mice. *Endocrinology* **154**, 698-708 (2013).

NCD Risk Factor Collaboration (NCD-RisC). Worldwide trends in underweight and obesity from 1990 to 2022: a pooled analysis of 3663 population-representative studies with 222 million children, adolescents, and adults. *Lancet* **403**, 1027-1050 (2024).

Nothnagel, P. M. C. *et al.* Transient SUMOylation inhibition in human pre-adipocytes stably imprints a transcriptional beiging fate. *Nucleic Acids Res.* **54**, (2026).

Paakinaho, V. *et al.* SUMOylation regulates the protein network and chromatin accessibility at glucocorticoid receptor-binding sites. *Nucleic Acids Res.* **49**, 1951-1971 (2021).

Patro, R., Duggal, G., Love, M. I., Irizarry, R. A. & Kingsford, C. Salmon provides fast and bias-aware quantification of transcript expression. *Nat. Methods* **14**, 417-419 (2017).

Paulsen, J. *et al.* Long-range interactions between topologically associating domains shape the four-dimensional genome during differentiation. *Nat. Genet.* **51**, 835-843 (2019).

Pimentel, H., Bray, N. L., Puente, S., Melsted, P. & Pachter, L. Differential analysis of RNA-seq incorporating quantification uncertainty. *Nat. Methods* **14**, 687-690 (2017).

PrimerQuest PCR & qPCR primer design tool. *Integrated DNA Technologies* https://eu.idtdna.com/PrimerQuest/Home/Index.

Pulit, S. L. *et al.* Meta-analysis of genome-wide association studies for body fat distribution in 694 649 individuals of European ancestry. *Hum. Mol. Genet.* **28**, 166-174 (2019).

Qian, H. *et al.* TET1 promotes RXRα expression and adipogenesis through DNA demethylation. *Biochim. Biophys. Acta Mol. Cell Biol. Lipids* **1866**, 158919 (2021).

*R: A Language and Environment for Statistical Computing. R Foundation for Statistical Computing*. (2025).

Rosenwald, M. & Wolfrum, C. The origin and definition of brite versus white and classical brown adipocytes. *Adipocyte* **3**, 4-9 (2014).

Rosonina, E., Akhter, A., Dou, Y., Babu, J. & Sri Theivakadadcham, V. S. Regulation of transcription factors by sumoylation. *Transcription* **8**, 220-231 (2017).

Sahin, U., de Thé, H. & Lallemand-Breitenbach, V. Sumoylation in physiology, pathology and therapy. *Cells* **11**, 814 (2022).

Saini, S. K., Mangalhara, K. C., Prakasam, G. & Bamezai, R. N. K. DNA Methyltransferase1 (DNMT1) Isoform3 methylates mitochondrial genome and modulates its biology. *Sci. Rep.* **7**, 1525 (2017).

Sapir, A. Not so slim anymore-evidence for the role of SUMO in the regulation of lipid metabolism. *Biomolecules* **10**, E1154 (2020).

Seeler, J.-S. & Dejean, A. SUMO and the robustness of cancer. *Nat. Rev. Cancer* **17**, 184-197 (2017).

Shah, A., Oldenburg, A. & Collas, P. A hyper-dynamic nature of bivalent promoter states underlies coordinated developmental gene expression modules. *BMC Genomics* **15**, 1186 (2014).

Shroff, T. *et al.* Studying metabolism with multi-organ chips: new tools for disease modelling, pharmacokinetics and pharmacodynamics. *Open Biol.* **12**, 210333 (2022).

Siersbæk, R. & Mandrup, S. Transcriptional networks controlling adipocyte differentiation. *Cold Spring Harb. Symp. Quant. Biol.* **76**, 247-255 (2011).

Siersbæk, R. *et al.* Dynamic rewiring of promoter-anchored chromatin loops during adipocyte differentiation. *Mol. Cell* **66**, 420-435.e5 (2017).

The Gene Ontology Consortium. The Gene Ontology knowledgebase in 2026. *Nucleic Acids Res* (2025).

Theurillat, I. *et al.* Extensive SUMO modification of repressive chromatin factors distinguishes pluripotent from somatic cells. *Cell Rep.* **32**, 108146 (2020).

Vinutha, H. P., Poornima, B. & Sagar, B. M. Detection of outliers using interquartile range technique from intrusion dataset. in *Advances in Intelligent Systems and Computing* 511-518 (Springer Singapore, Singapore, 2018).

Walsh, C. T., Garneau-Tsodikova, S. & Gatto, G. J., Jr. Protein posttranslational modifications: the chemistry of proteome diversifications. *Angew. Chem. Int. Ed Engl.* **44**, 7342-7372 (2005).

Wen, W. *et al.* Dynamic rendition of adipose genes under epigenetic regulation: Revealing new mechanisms of obesity occurrence. *Curr. Issues Mol. Biol.* **47**, 540 (2025).

Obesity and overweight. *Who.int* https://www.who.int/news-room/fact-sheets/detail/obesity-and-overweight.

Wronska, A. & Kmiec, Z. Structural and biochemical characteristics of various white adipose tissue depots. *Acta Physiol. (Oxf.)* **205**, 194-208 (2012).

Wu, L., Wang, X., Wang, L., Li, S. & Chen, Q. DNA methylation and demethylation in adipocyte biology: roles of DNMT and TET proteins in metabolic disorders. *Front. Endocrinol. (Lausanne)* **16**, 1591152 (2025).

Xu, F. *et al.* Epigenetic induction of tumor stemness via the lipopolysaccharide-TET3-HOXB2 signaling axis in esophageal squamous cell carcinoma. *Cell Commun. Signal.* **18**, 17 (2020).

Yang, X. *et al.* DNA methylation biphasically regulates 3T3-L1 preadipocyte differentiation. *Mol. Endocrinol.* **30**, 677-687 (2016).

Ye, J. *et al.* Primer-BLAST: a tool to design target-specific primers for polymerase chain reaction. *BMC Bioinformatics* **13**, 134 (2012).

Zhao, X. *et al.* Waves of sumoylation support transcription dynamics during adipocyte differentiation. *Nucleic Acids Res.* **50**, 1351-1369 (2022).

Zhou, X. *et al.* OGG1 is essential in oxidative stress induced DNA demethylation. *Cell. Signal.* **28**, 1163-1171 (2016).

# 7. Supplementals

| Name | Sequence (5' → 3') | Reference |
|---|---|---|
| DNMT1_Primer1_f | AGACAAGTTACTAGGAGGAGACA | This study |
| DNMT1_Primer1_r | GAATCAGTTATGTGACTTGGAAACC | |
| DNMT1_Primer2_f | GGTTTCCTTCCTCAGCTACTGCGA | Liao *et al.*, 2020 |
| DNMT1_Primer2_r | CACTGATAGCCCATGCGGACCA | |
| DNMT3A_Primer1_f | GACTCCATCACGGTGGGCATGG | Liao *et al.*, 2020 |
| DNMT3A_Primer1_r | TGTCCCTCTTGTCACTAACGCC | |
| DNMT3A_Primer2_f | TCCACTGTGAATGATAAGCTG | Liao *et al.*, 2020 |
| DNMT3A_Primer2_r | GGAAACCAAATACCCTTTCCA | |
| DNMT3B_Primer1_f | GAGTCCATTGCTGTTGGAACCG | Liao *et al.*, 2020 |
| DNMT3B_Primer1_r | ATGTCCCTCTTGTCGCCAACCT | |
| DNMT3B_Primer2_f | GACTGCTTGGAATACAATAGGA | Liao *et al.*, 2020 |
| DNMT3B_Primer2_r | AAAGCCAAAGATCCTTTCGAG | |
| TET1_Primer1_f | CCCTATGCAATTCTGTAAAGC | This study |
| TET1_Primer1_r | AGCAACACTTGGTCCTG | |
| TET1_Primer2_f | GCAGCGTACAGGCCACCACT | Xu *et al.*, 2020 |
| TET1_Primer2_r | AGCCGGTCGGCCATTGGAAG | |
| TET2_Primer1_f | CCTACATTTAAGTATCCTCACTAGCC | This study |
| TET2_Primer1_r | TGCATGACTGGTCCTGAAAG | |
| TET2_Primer2_f | TTCGCAGAAGCAGCAGTGAAGAG | Xu *et al.*, 2020 |
| TET2_Primer2_r | AGCCAGAGACAGCGGGATTCCTT | |
| TET3_Primer1_f | GACGAGAACATCGGCGGCGT | Xu *et al.*, 2020 |
| TET3_Primer1_r | GTGGCAGCGGTTGGGCTTCT | |
| CEBPA | GACTTGGTGCGTCTAAGATGAG | Nothnagel *et al.,* 2026 |
| CEBPA | GGCATTGGAGCGGTGAGTT | |
| 18S_f | GCAGAATCCACGCGCCAGTACAAG | Nothnagel *et al.,* 2026 |
| 18S_r | GCTTGTTGTCCAGACCATTGGC | |

***Table S1. RT-qPCR primer sequences.*** *List of primer sequences used for quantitative RT-qPCR analysis of DNMTs, TETs, CEBPA and housekeeping gene 18S.*

| Antibody | Supplier | Cat. Number | Dilution |
|---|---|---|---|
| DNMT1 | Abcam | ab13537 | 1:1000 |
| DNMT3A | Abcam | ab2850 | 1:500 |
| DNMT3B | Abcam | ab2850 | 1:500 |
| TET1 | Abcam | ab191698 | 1:500 |
| TET2 | Cell Signaling Technology | 18950S | 1:500 |
| TET3 | Cell Signaling Technology | 99980 | 1:500 |
| γ-Tubulin | Sigma-Aldrich | T5326-100UL | 1:1000 |
| Anti-Rabbit IgG HRP | Amersham | NA934-1ML | 1:10000 |
| Anti-mouse IgG HRP | GE | NA931V | 1:10000 |

***Table S2. Antibodies****. List of primary and secondary antibodies used for western blot analysis of DNMTs and TETs. γ-Tubulin was used as loading control.*

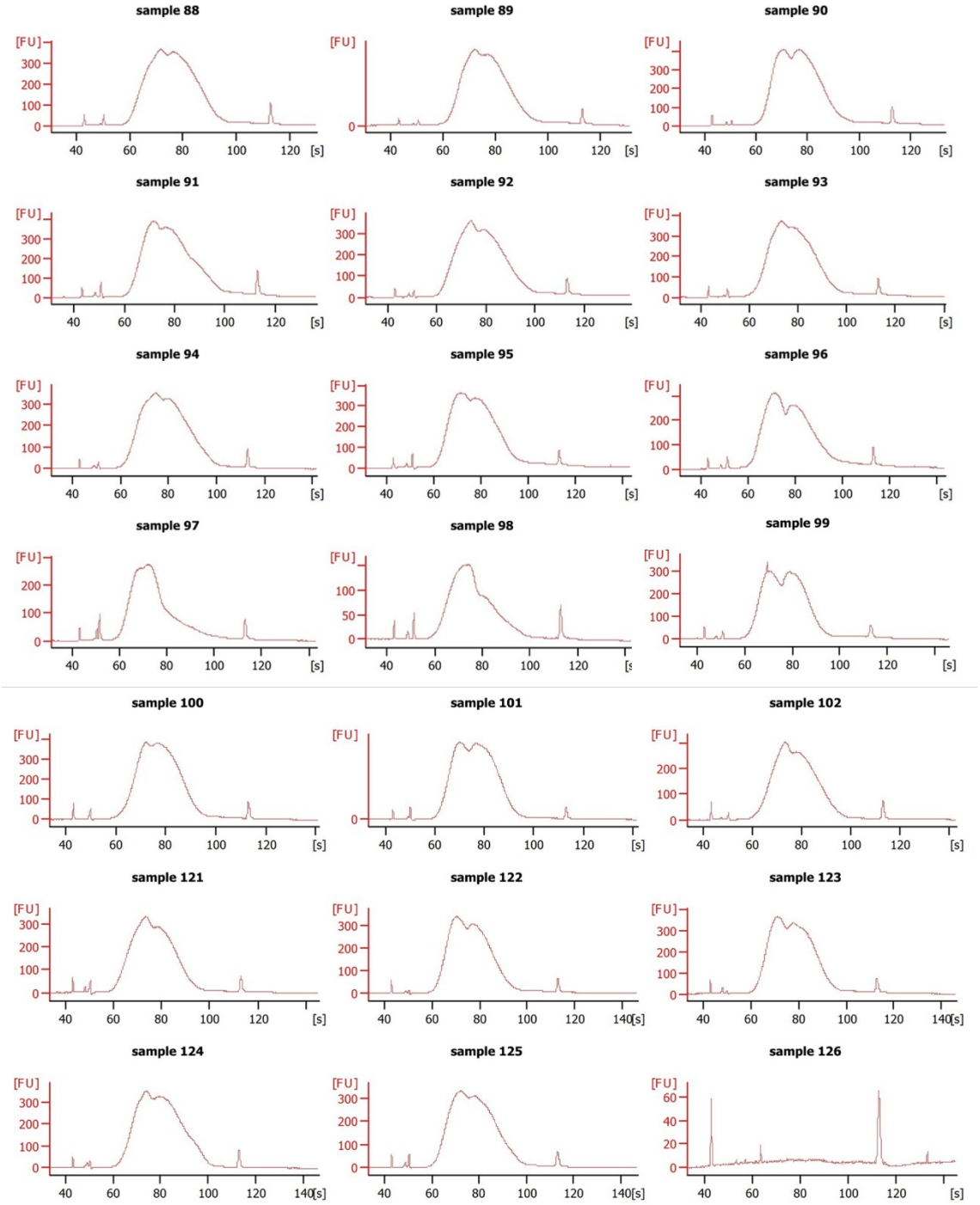


***Figure S1. Bioanalyzer electropherograms of EM-seq library preparations.*** *Libraries were generated from samples collected at day −2 (samples 88-90, no treatment), day 0 (samples 91-93, DMSO; 94-96, TAK-981), 12 h (samples 97-99, DMSO; 100-102, TAK-981) and day 7 (samples 121-123, DMSO; 124-126, TAK-981).The electropherograms show the fragment size distribution and quality of the prepared libraries prior to sequencing.*